REPORT NO.
UCB/SEMM-91/08

STRUCTURAL ENGINEERING,
MECHANICS AND MATERIALS

APPLICATION OF A RETURN MAP ALGORITHM TO PLASTICITY AND VISCO-PLASTICITY MODELS

by

FERDINANDO AURICCHIO

ROBERT L. TAYLOR

and

JACOB LUBLINER

November 1991

DEPARTMENT OF CIVIL ENGINEERING
UNIVERSITY OF CALIFORNIA
BERKELEY, CALIFORNIA

APPLICATION OF A RETURN MAP ALGORITHM TO PLASTICITY AND VISCO-PLASTICITY MODELS

F.Auricchio R.L.Taylor
J.Lubliner
Department of Civil Engineering, University of California at Berkeley, Berkeley, CA 94720 USA

Abstract

This work deals with the computational analysis of non-linear *associative generalized* plasticity and visco-plasticity material models. After a brief review of the continuous equations governing the behavior of such models, including both linear isotropic and kinematic hardening mechanisms, we introduce their discrete counterpart within the framework of a *return mapping* algorithm. We also address a simple and efficient approach for the construction of the *consistent* tangent matrix, which guarantees quadratic convergence in a Newton iterative technique. The numerical implementation of some material models in which the inelastic behavior is based upon a von Mises surface is analyzed in detail; we consider the well known classical plasticity and visco-plasticity models and recently proposed generalized plasticity and generalized visco-plasticity models [17, 18]. The generalized plasticity model shows some new and interesting features such as: they *smoothly* reach a limiting asymptote for both monotonic and cyclic loading conditions; if unloaded in the plastic range, upon reloading, they show renewed plasticity before the attainment of the stress where unloading began. Some numerical simulations are presented to show the performance and the differences between the models. In particular, the comparison with the analytical solution is reported for a thin walled tube subjected to tension and torsion under load control.

1. Introduction

The development of non-linear material models represents an area where considerable efforts are directed in an attempt to simulate the behavior of real materials in a more complete form. Consequently, topics still widely addressed are the implementation of non-linear models including all the related computational aspects, such as the method of integration of rate type constitutive equations.

The objective of this work is to: review classical plasticity and visco-plasticity models and *generalized* plasticity and visco-plasticity models, discussing their numerical implementation in the framework of a return mapping algorithm; address a simple and efficient approach

for the construction of the *consistent* tangent matrix for an associative J2 material model, including both isotropic and kinematic hardening mechanisms.

The work is organized as follow. In Section 2 we introduce the generalized constitutive equations for a non-linear material with a von Mises yield function and an associative flow rule. The model includes both linear isotropic and kinematic hardening mechanisms, and the capability to have a limit equation different from the yield function, such as in the *generalized* models. In Section 3 we present the discrete version of the equations introduced in Section 2, with a brief review of the *return mapping* algorithm used for their integration. In Section 4 the discrete equations and the integration algorithm are specialized to various models. In Section 5 we address the construction of the tangent matrix, such that it is consistent with the discrete version of the equations. The use of a consistent tangent matrix guarantees quadratic convergence in the application of a Newton iterative algorithm. In Section 6 the tangent matrix is specialized to the models already discussed in Section 4. Among others, we look at the well known classical plasticity and classical visco-plasticity models, and at the recently introduced and discussed generalized plasticity and generalized visco-plasticity models [17, 18]. The generalized models are of particular interest since they show some new and interesting features: they *smoothly* reach a limiting asymptote for both monotonic and cyclic loading conditions; if unloaded from the plastic range, upon reloading, they show renewed plasticity before the attainment of the stress where unloading began. In the last section we present some numerical simulations using a finite element implementation to show the performance and the differences between the models. In addition to some more classical examples, such as as a simple tension test and a thick tube under internal pressure, we present the results obtained for a thin tube subjected to tension and torsion: first, where loading is applied by controlling the strains, and second by controlling the stresses. For this latter case the numerical solution is compared to a closed form solution derived for the generalized plasticity model.

2. Constitutive equations for an associative J2 material

In this section we consider the equations governing the behavior of an inelastic material, controlled by the second invariant of the deviatoric stress, J_2 (a von Mises type model), and an associative flow rule. We shall refer to this general class as J2 models or J2 materials. The model includes both linear isotropic and kinematic hardening mechanisms, which are controlled by the two parameters H_{iso} and H_{kin}, and the back stress tensor, $\boldsymbol{\alpha}$.

Based on the assumption of J2 material, the evolution equations involve only the deviatoric stress and strain, $\mathbf{s}$ and $\mathbf{e}$ respectively. If we denote the total stress as $\boldsymbol{\sigma}$ and the total strain as $\boldsymbol{\epsilon}$, the following relations hold:

$$\boldsymbol{\sigma} = \frac{1}{3}\mathrm{tr}(\boldsymbol{\sigma})\mathbf{1} + \mathbf{s} \tag{1}$$

$$\boldsymbol{\epsilon} = \frac{1}{3}\mathrm{tr}(\boldsymbol{\epsilon})\mathbf{1} + \mathbf{e} \tag{2}$$

$\mathbf{1}$ is the second order unit tensor and $\mathrm{tr}(\cdot)$ is the trace operator (i.e. $\mathrm{tr}(\boldsymbol{\sigma}) = \mathbf{1} : \boldsymbol{\sigma}$). The linear vector space of second order tensors is equipped with the natural (Euclidean) inner

product, defined by the trace of the product of two tensors:

$$\|\mathbf{a}\|^2 = \mathbf{a} : \mathbf{a} = \mathrm{tr}(\mathbf{a} \cdot \mathbf{a}) \tag{3}$$

$\mathbf{a}$ is any second order tensor. We note that: $\|\mathbf{s}\| = \sqrt{2J_2}$.

Assuming an additive decomposition of the strain into elastic and plastic part:

$$\boldsymbol{\epsilon} = \boldsymbol{\epsilon}^{el} + \boldsymbol{\epsilon}^{p} \tag{4}$$

and denoting the time as t, the governing equations are:

$$\mathbf{s}(t) = 2G\left(\mathbf{e}(t) - \mathbf{e}^{p}(t)\right) = 2G\mathbf{e}^{el}(t) \tag{5}$$

$$\boldsymbol{\Sigma} = \mathbf{s} - \boldsymbol{\alpha} \tag{6}$$

$$f\left(\boldsymbol{\Sigma}(t), \sigma_y(t)\right) = \|\boldsymbol{\Sigma}(t)\| - \sqrt{\frac{2}{3}}\sigma_y(t) \tag{7}$$

$$g\left(f(t), \boldsymbol{\xi}(t), \dot{\gamma}(t)\right) \leq 0 \tag{8}$$

$$\dot{\mathbf{e}}^{p}(t) = \dot{\gamma}(t)\frac{\partial f(t)}{\partial \boldsymbol{\Sigma}(t)} \tag{9}$$

$$\dot{\boldsymbol{\alpha}}(t) = \frac{2}{3}H_{kin}\dot{\mathbf{e}}^{p}(t) \tag{10}$$

Equation (5) is the linear elastic relation between the deviatoric stress $\mathbf{s}(t)$ and the elastic deviatoric strain $\mathbf{e}^{el}(t)$; $\mathbf{e}(t)$ and $\mathbf{e}^{p}(t)$ are the deviatoric part of the total strain and of the plastic strain, respectively.

Equation (6) is merely the definition of the *relative* stress $\boldsymbol{\Sigma}$, since the back stress $\boldsymbol{\alpha}$ physically represents the center of the yield surface, which can shift as a result of the kinematic hardening mechanism.

Equation (7) is the von Mises yield function where: $\sigma_y(t)$ is the yield stress in uniaxial tension, whose time dependence is due to an isotropic hardening mechanism, which in the simplest form is given by:

$$\sigma_y(t) = \sigma_{y0} + H_{iso}\,\bar{e}^{p}(t) \tag{11}$$

σ_{y0} is the initial uniaxial yield stress and $\bar{e}^{p}$ is the equivalent plastic strain:

$$\bar{e}^{p}(t) = \int_0^t \sqrt{\frac{2}{3}}\|\dot{\mathbf{e}}(t)\|dt \tag{12}$$

Equation (8) is the limit equation expressed in terms of the yield function f, a set of internal variable $\boldsymbol{\xi}(t)$ and a *consistency parameter* $\dot{\gamma}(t)$, that is required to be greater or equal to zero. It embodies and models the rate dependency and the yielding characteristic of a material. Observe that the yield equation and the yield function are not required to be the same, i.e. g and f coincide only if some simplifications apply to the model (for example, in classical plasticity, $g = f = 0$). In the above the operation $\dot{(\cdot)}$ indicates a derivative with respect to the independent time variable t; in the case of a rate independent material, t is a fictitious

time introduced only to describe an evolutionary process. In this work we consider the following four specific forms for equation (8):

a) classical plasticity	$g = f = \|\boldsymbol{\Sigma}(t)\| - \sqrt{\frac{2}{3}}\sigma_y(t) = 0$	(13)
b) classical visco-plasticity	$g = \Phi\left[\frac{f}{R_0}\right] - \frac{\eta}{R_0}\dot{\gamma} = 0$	(14)
c) generalized plasticity	$g = \dot{\gamma} - h(\mathbf{n}^* : \dot{\boldsymbol{\sigma}}) = 0$	(15)
d) generalized visco-plasticity	$g = \dot{\gamma} - (h\ \mathbf{n}^* : \dot{\boldsymbol{\sigma}}) - \frac{R_0}{\eta}\ \Phi\left[\frac{f}{R_0}\right] = 0$	(16)

These models are described more completely in Section 4.
Equation (9) is the evolution equation (flow rule) for the deviatoric plastic strain, in the framework of *associative* plasticity.
Equation (10) is the simplest form of the Prager equation for the evolution of the back stress $\boldsymbol{\alpha}(t)$.
Since we limit ourselves to the case of von Mises yield function, the following equalities hold:

$$\frac{\partial f(t)}{\partial \boldsymbol{\Sigma}(t)} = \frac{\boldsymbol{\Sigma}(t)}{\|\boldsymbol{\Sigma}(t)\|} = \mathbf{n}(t) \tag{17}$$

where $\mathbf{n}(t)$ is the tensor normal to the yield function at $\boldsymbol{\Sigma}$ and having unit norm. As a result, equation (9) and (10) can be rewritten as:

$$\dot{\mathbf{e}}^p = \dot{\gamma}(t)\mathbf{n}(t) \tag{18}$$

$$\dot{\boldsymbol{\alpha}}(t) = \frac{2}{3}H_{kin}\dot{\gamma}(t)\mathbf{n}(t) \tag{19}$$

The above briefly presents the equations governing the behavior of an associative J2 material; a more rigorous and general approach can be found in Reference 1 and 2.

3. Discrete constitutive equations and integration algorithm

From a computational standpoint we treat the non-linear behavior of a material as a strain driven problem. This means that the stress history is obtained from the strain history by means of an integration technique, such as a *return mapping* algorithm. Therefore, in this section we introduce a discrete version of the equations presented earlier and review the integration algorithm.

Let $[0, T] \subset R$ be the time interval of interest and consider two time values within it, say t_n and $t_{n+1} > t_n$, such that t_{n+1} is the first time value of interest after t_n. To make the equations more readable, we introduce the following convention:

$$\mathbf{a}_n = \mathbf{a}(t_n)\ ,\quad \mathbf{a} = \mathbf{a}(t_{n+1}) \tag{20}$$

where $\mathbf{a}$ is any generic quantity. According to this notation, in the discrete version of the equations the subscript n indicates a quantity that is evaluated at time t_n, while no subscript indicates a quantity that is evaluated at time t_{n+1}.

We assume that the solution at time t_n is known and given by the state:

$$\{\mathbf{s}_n, \mathbf{e}_n, \mathbf{e}_n^p, \boldsymbol{\alpha}_n, \overline{e}_n^p\} \tag{21}$$

We wish to compute the solution for the state at time t_{n+1} assuming that the total strain ϵ at time t_{n+1} is also given. Using the backward Euler integration formula [5, 6] for the plastic strain and for the back stress flow rules, we obtain:

$$\mathbf{e}^p = \mathbf{e}_n^p + \sqrt{\frac{2}{3}}\,\lambda\,\mathbf{n} \tag{22}$$

$$\boldsymbol{\alpha} = \boldsymbol{\alpha}_n + \frac{2}{3} H_{kin}\,\lambda\,\mathbf{n} \tag{23}$$

where:

$$\lambda = \int_{t_n}^{t_{n+1}} \dot{\gamma}(t)dt \tag{24}$$

Substitution of (22) into (5) yields:

$$\mathbf{s} = 2G\,(\mathbf{e} - \mathbf{e}_n^p) - 2G\,\lambda\,\mathbf{n} \tag{25}$$

while subtracting (23) from (25) gives:

$$\boldsymbol{\Sigma} = \mathbf{s} - \boldsymbol{\alpha} = 2G\,(\mathbf{e} - \mathbf{e}_n^p) - \boldsymbol{\alpha}_n - \left(2G + \frac{2}{3} H_{kin}\right)\lambda\,\mathbf{n} \tag{26}$$

Equations (22), (23) and (25) represent the discrete counterpart of equations (9), (10) and (5), respectively. Here λ is an unknown quantity and is computed by means of the integration algorithm.

Initially suggested by Maenchen and Sack [3] and Wilkins [4], the return mapping algorithm provides an efficient and robust integration scheme, based on a discrete enforcement of the limit equation. It belongs to the family of elastic-predictor plastic-corrector algorithms and, hence, is a two part algorithm. In the first part, a purely elastic *trial state* is computed; in the second, if the trial state violates any of the constitutive equations, a correction is computed and applied in a manner that the final state is consistent with the discrete constitutive model. The algorithm has been widely studied [7, 8, 9] as has its stability [10, 11, 12]. It has also been extended to several problems of interest, which include the plane-stress problem [13] and models with multi-surface yield functions [14]. It is interesting to recall that the incremental elasto-plastic initial value problem can be reformulated as a constrained convex minimization problem, which is a discrete counterpart of the classical *maximum plastic dissipation* postulate. Using this analogy, the return mapping algorithm can be shown to be the closest point projection of the trial state to the limit surface $g = 0$. Therefore, besides its simplicity, this algorithm has a very strong theoretical basis. Details of this analogy and theoretical discussions can be found in [15]. For the particular case of J2 associative materials, the search for the closest point reduces to a radial return mapping.

We shall now discuss the two steps of the algorithm in more detail.

- *Trial state*: we assume that in the interval $[t_n, t_{n+1}]$ no plastic deformation occurs (i.e. $\mathbf{e}^p = \mathbf{e}_n^p$, which implies: $\lambda = 0$, $\boldsymbol{\alpha} = \boldsymbol{\alpha}_n$). As a result, we have:

$$\mathbf{s}^{TR} = 2G(\mathbf{e} - \mathbf{e}_n^p) \tag{27}$$

$$\mathbf{e}^{p,TR} = \mathbf{e}^{p}_{n} \tag{28}$$

$$\boldsymbol{\alpha}^{TR} = \boldsymbol{\alpha}_{n} \tag{29}$$

$$\boldsymbol{\Sigma}^{TR} = \mathbf{s}^{TR} - \boldsymbol{\alpha}^{TR} = \mathbf{s}^{TR} - \boldsymbol{\alpha}_{n} \tag{30}$$

If the elastic trial state is admissible, i.e. it does not violate the limit equation (8), then it represents the solution at time t_{n+1}. Consequently, the solution can be updated with the trial state and the second part of the algorithm is skipped.

- *Plastic correction*: if the trial state is not admissible, a correction has to be performed. Enforcing the satisfaction of the limit equation, the consistency parameter λ may be computed, as shown for some specific material models in Section 4. Equations (25) and (26) can be now rewritten in terms of the trial state and λ:

$$\mathbf{s} = \mathbf{s}^{TR} - 2G\,\lambda\,\mathbf{n} \tag{31}$$

$$\boldsymbol{\Sigma} = \boldsymbol{\Sigma}^{TR} - \left(2G + \frac{2}{3}H_{kin}\right)\,\lambda\,\mathbf{n} \tag{32}$$

which allows us to compute and update the solution.

From equation (17) we have:

$$\boldsymbol{\Sigma} = \|\boldsymbol{\Sigma}\|\,\mathbf{n} \tag{33}$$

hence from equation (32) we deduce that:

$$\boldsymbol{\Sigma}^{TR} = \|\boldsymbol{\Sigma}^{TR}\|\,\mathbf{n} \tag{34}$$

or that:

$$\mathbf{n} = \mathbf{n}^{TR} \tag{35}$$

and the following scalar relation between $\|\boldsymbol{\Sigma}\|$ and $\|\boldsymbol{\Sigma}^{TR}\|$ can be obtained:

$$\|\boldsymbol{\Sigma}\| = \|\boldsymbol{\Sigma}^{TR}\| - \left(2G + \frac{2}{3}H_{kin}\lambda\right) \tag{36}$$

Equations (33-36) represent a radial return mapping since all the tensor quantities which appear are associated with the same $\mathbf{n}$. Therefore, $\|\boldsymbol{\Sigma}\|$ and $\boldsymbol{\Sigma}$ may be easily compute, once λ is determined.

4. Discrete plasticity and visco-plasticity models

In this section we show how different material models can be treated within the framework of the return mapping algorithm. In particular, we discuss the implementation of the well known classical plasticity and classical visco-plasticity models, and the recently introduced generalized plasticity and generalized visco-plasticity models [17, 18].

As a result of equation (36) in Section 3, the application of the return mapping algorithm to different material models requires the evaluation of the discrete consistency parameter. Since λ measures the correction that renders a non-admissible trial state admissible, it must be computed enforcing the discrete version of the appropriate limit equation.

4.1. Classical plasticity

In classical plasticity, the limit equation coincides with the yield function:

$$g = f = \|\boldsymbol{\Sigma}(t)\| - \sqrt{\frac{2}{3}}\sigma_y(t) = 0 \tag{37}$$

and in a discrete form it can be written as:

$$\|\boldsymbol{\Sigma}\| - R = 0 \tag{38}$$

where R is the radius of the yield surface:

$$\begin{aligned} R &= R(t_{n+1}) = \sqrt{\frac{2}{3}}\sigma_y(t_{n+1}) \\ &= \sqrt{\frac{2}{3}}\left[\sigma_{y0} + H_{iso}\,\bar{e}^p\right] \\ &= \sqrt{\frac{2}{3}}\left[\sigma_{y0} + H_{iso}\,\bar{e}^p_n + H_{iso}\,(\bar{e}^p - \bar{e}^p_n)\right] \\ &= R_n + \frac{2}{3}H_{iso}\,\lambda \end{aligned} \tag{39}$$

Recalling the scalar relation between $\|\boldsymbol{\Sigma}^{TR}\|$ and $\|\boldsymbol{\Sigma}\|$, equation (37) can be written as:

$$\left[\|\boldsymbol{\Sigma}^{TR}\| - \left(2G + \frac{2}{3}H_{kin}\right)\lambda\right] - \left(R_n + \frac{2}{3}H_{iso}\lambda\right) = 0 \tag{40}$$

Thus, solving for λ, we obtain:

$$\lambda = \frac{\|\boldsymbol{\Sigma}^{TR}\| - R_n}{2G_1} \tag{41}$$

where:

$$G_1 = G + \frac{1}{3}(H_{kin} + H_{iso}) \tag{42}$$

4.2. Classical visco-plasticity

We consider a visco-plasticity model due to Perzyna [16]. The limit equation is:

$$g = \Phi\left[\frac{f}{R_0}\right] - \frac{\eta}{R_0}\dot{\gamma} = 0 \tag{43}$$

where Φ is a function deduced by dynamic tests on the material, R_o is the initial radius of the yield surface and η plays the role of a viscosity. The function $\Phi(x)$ is commonly chosen to be x^m, such that the model yields:

$$\left[\frac{f}{R_0}\right]^m - \frac{\eta}{R_0}\dot{\gamma} = 0 \tag{44}$$

Integrating with respect to time using a backward Euler method, we obtain:

$$\left[\frac{f}{R_0}\right]^m \Delta t - \frac{\eta}{R_0}\lambda = 0 \tag{45}$$

and, introducing the discrete relations of Section 3:

$$\left[\frac{(\|\boldsymbol{\Sigma}^{TR}\| - R_n) - 2G_1\lambda}{R_0}\right]^m \Delta t - \frac{\eta}{R_0}\lambda = 0 \tag{46}$$

For $m = 1$ and $m = 2$, the parameter λ can be computed in closed form; for $m > 2$ an iterative technique for the solution of the non-linear equation may be implemented. We regain the classical plasticity consistency parameter for $\eta \to 0$.

4.3. Generalized plasticity

A simple model of generalized plasticity was introduced by Lubliner in Reference 17 and extended by the authors in Reference 18. Referring to the notation of this last work, the yield equation is:

$$g = \dot{\gamma} - h\,(\mathbf{n}^* : \dot{\boldsymbol{\sigma}}) = 0 \tag{47}$$

where:

$$h = \frac{f}{\zeta(r - f) + \frac{2}{3}Hr} \quad , \quad \mathbf{n}^* = \frac{\partial f}{\partial \boldsymbol{\sigma}} \tag{48}$$

with r and ζ two positive constants with dimensions of stress and $H = H_{iso} + H_{kin}$. The parameters β and δ used in Reference 18 are related to r and ζ by the relations:

$$r = \sqrt{\frac{2}{3}}\beta \quad , \quad \zeta = \frac{2}{3}\delta \tag{49}$$

in fact β measures how much the asymptotic limit exceeds the yield stress σ_y in uniaxial tension/compression, while r measures the analogous quantity with respect to R but in a three dimensional setting. The parameter ζ has an analogous meaning with respect to δ.

Before computing the parameter λ, the term $(\mathbf{n}^* : \dot{\boldsymbol{\sigma}})$ may be simplified, since we are considering a J2 material. Accordingly, we have:

$$\mathbf{n}^* = \frac{\partial f}{\partial \boldsymbol{\Sigma}}\frac{\partial \boldsymbol{\Sigma}}{\partial \boldsymbol{\sigma}} = \mathbf{n}\frac{\partial \mathbf{s}}{\partial \boldsymbol{\sigma}} = \mathbf{n} \tag{50}$$

due to the fact that $\boldsymbol{\alpha}$ is an independent variable. Therefore:

$$\begin{aligned}
\mathbf{n}^* : \dot{\boldsymbol{\sigma}} &= \mathbf{n} : \dot{\boldsymbol{\sigma}} = \mathbf{n} : (\dot{p}\,\mathbf{1} + \dot{\mathbf{s}}) \\
&= \dot{p}\,\mathrm{tr}(\mathbf{n}) + \mathbf{n} : \dot{\mathbf{s}} \\
&= \mathbf{n} : \dot{\mathbf{s}} = \mathbf{n} : \dot{\boldsymbol{\Sigma}} + \mathbf{n} : \dot{\boldsymbol{\alpha}} \\
&= \mathbf{n} : \dot{\boldsymbol{\Sigma}} + \mathbf{n} : \left(\frac{2}{3}\dot{\gamma}H_{kin}\mathbf{n}\right) \\
&= \mathbf{n} : \dot{\boldsymbol{\Sigma}} + \frac{2}{3}\dot{\gamma}H_{kin}
\end{aligned} \tag{51}$$

Since:

$$(\mathbf{n} : \mathbf{n}) = 1 \quad \Rightarrow \quad (\mathbf{n} : \dot{\mathbf{n}}) = (\dot{\mathbf{n}} : \mathbf{n}) = 0 \tag{52}$$

equation (51) can be simplified as follow:

$$\mathbf{n}^* : \dot{\boldsymbol{\sigma}} \;=\; \mathbf{n} : \dot{\boldsymbol{\Sigma}} + \frac{2}{3}\dot{\gamma}H_{kin}$$

$$
\begin{aligned}
&= \mathbf{n} : \frac{d}{dt}(\|\boldsymbol{\Sigma}\|\mathbf{n}) + \frac{2}{3}\dot{\gamma} H_{kin} \\
&= \|\boldsymbol{\Sigma}\| (\mathbf{n} : \dot{\mathbf{n}}) + (\mathbf{n} : \mathbf{n}) \frac{d}{dt}\|\boldsymbol{\Sigma}\| + \frac{2}{3}\dot{\gamma} H_{kin} \\
&= \frac{d}{dt}\|\boldsymbol{\Sigma}\| + \frac{2}{3}\dot{\gamma} H_{kin} \qquad (53)
\end{aligned}
$$

As a result, for a J2 material the limit equation (47) can be rewritten as:

$$
\dot{\gamma} - h\left[\frac{d}{dt}\|\boldsymbol{\Sigma}\| + \frac{2}{3}\dot{\gamma} H_{kin}\right] = 0 \qquad (54)
$$

Integrating over the time interval $[t_n, t_{n+1}]$, we obtain:

$$
\lambda - h\left[\|\boldsymbol{\Sigma}\| - \|\boldsymbol{\Sigma}_n\| + \frac{2}{3}\lambda\, H_{kin}\right] = 0 \qquad (55)
$$

and, introducing the discrete equations (36), we can finally solve for λ. If we set:

$$
\begin{aligned}
A_1 &= \|\boldsymbol{\Sigma}^{TR}\| - R_n \\
A_2 &= \|\boldsymbol{\Sigma}^{TR}\| - \|\boldsymbol{\Sigma}_n\| \\
A_3 &= \zeta - 2G \\
A_4 &= \left(\zeta + \frac{2}{3}H\right) r \qquad (56)
\end{aligned}
$$

we obtain the quadratic equation:

$$
a\lambda^2 + b\lambda + c = 0 \qquad (57)
$$

where:

$$
\begin{aligned}
a &= 2G_1 A_3 \\
b &= A_4 - A_1 A_3 + 2G_1 A_2 \\
c &= -A_1 A_2 \qquad (58)
\end{aligned}
$$

The physically correct solution to this equation corresponds to the smallest positive root.

If $\beta = r = 0$, then the discrete model must recover the classical plasticity case. Since $r = 0$, $A_4 = 0$ and $\|\boldsymbol{\Sigma}_n\| \leq \|\boldsymbol{\Sigma}\|$, which implies $A_2 \geq A_1$. Equation (57) reduces to:

$$
(2G_1 A_3)\,\lambda^2 + (-A_1 A_3 + 2G_1 A_2)\,\lambda - A_1 A_2 = 0 \qquad (59)
$$

which can be rewritten as:

$$
(2G_1\lambda - A_1)\ (A_3\lambda + A_2) = 0 \qquad (60)
$$

which has the following roots:

$$
\lambda_1 = -\frac{A_2}{A_3}\ , \qquad \lambda_2 = \frac{A_1}{2G_1} \qquad (61)
$$

The first root never represents the correct one: in fact for $\zeta > 2G$ it is negative and, therefore, violates the model; for $0 \leq \zeta < 2G$, we have $\lambda_1 > \lambda_2$. On the other hand, the second root

is always physically correct and coincides with the root of the classical plasticity model. Therefore, for $r = 0$ the discrete generalized plasticity model always reduces to the classical one, as expected.

If $\zeta = 0$ and the hardening is also zero, then equation (60) becomes:

$$(2G\lambda - A_1)\ (-2G\lambda + A_2) = 0 \tag{62}$$

which has the roots:

$$\lambda_1 = \frac{A_2}{2G} \quad \geq \quad \lambda_2 = \frac{A_1}{2G} \tag{63}$$

Again the second root coincides with the classical plasticity root and it can be proven by induction that $A_2 \geq A_1$ also for this case.

It is interesting to observe that in the classical visco-plastic model an admissible inelastic state of stress can be outside the surface $f = 0$; but it must always be on the surface $g = 0$. Since the return mapping algorithm is such that the trial state is projected on the limit equation surface, we observe that the condition $\lambda > 0$ is sufficient to determine if a step is non-elastic. In theoretical works, the determination of an inelastic step also requires that: $(\boldsymbol{\Sigma} : d\mathbf{e} > 0)$. Within the return mapping algorithm, this latter condition is already embedded in the determination of λ and therefore is automatically accounted for when we project the trial state onto the limit equation.

4.4. Generalized visco-plasticity

We refer to the simple generalized visco-plasticity model introduced and discussed in [18]. The limit equation can be written as:

$$g = \dot{\gamma} - h\ (\mathbf{n}^* : \dot{\boldsymbol{\sigma}}) - \frac{R_0}{\eta}\,\Phi\left[\frac{f}{R_0}\right] = 0 \tag{64}$$

where again:

$$h = \frac{f}{\zeta(r - f) + \frac{2}{3}Hr} \quad , \quad \mathbf{n}^* = \frac{\partial f}{\partial \boldsymbol{\sigma}} \tag{65}$$

Note that for $\eta \to 0$ equation (64) is equivalent to the classical plasticity model, while for $\eta \to \infty$ it goes to the generalized plasticity model. For a generic value of η between 0 and ∞, we get a generalized visco-plasticity material.

Assuming $\Phi(x) = x$ and using the result derived in Section 4.3, equation (64) can be rewritten as:

$$\dot{\gamma} - \left[h\left(\frac{d}{dt}\|\boldsymbol{\Sigma}\| + \frac{2}{3}H_{kin}\dot{\gamma}\right) + \frac{f}{\eta}\right] = 0 \tag{66}$$

Integrating with respect to time, we obtain:

$$\lambda - \left[h\left(\|\boldsymbol{\Sigma}\| - \|\boldsymbol{\Sigma}_n\| + \frac{2}{3}H_{kin}\lambda\right) + \frac{f}{\eta}\Delta t\right] = 0 \tag{67}$$

Introducing the discrete equations discussed in Section 3 and using position (56), we end up again with a quadratic equation:

$$a\lambda^2 + b\lambda + c = 0 \tag{68}$$

where:

$$\begin{aligned} a &= 2G_1\left[A_3 + 2G_1\frac{\Delta t}{\eta}\zeta\right] \\ b &= A_4 - A_1A_3 + 2G_1A_2 + 2G_1\frac{\Delta t}{\eta}(A_4 - 2A_1\zeta) \\ c &= -A_1A_2 - \frac{\Delta t}{\eta}A_1(A_4 - A_1\zeta) \end{aligned} \tag{69}$$

Also starting from equation (68) we regain the classical plasticity solution for $\eta \to 0$ and the generalized plasticity solution for $\eta \to \infty$, as expected.

5. Consistent algorithmic tangent moduli

In this section we address a simple and efficient approach for constructing the tangent matrix, in a form consistent with the discrete version of the constitutive equations described in the previous sections. The use of a consistent tangent matrix preserves the quadratic convergence of a Newton method, which we adopt in Section 7 for the incremental solution of the models using a finite element method.

For an arbitrary function $z(\mathbf{x})$, the tangent value in term of the increment $d\mathbf{x}$ of its variable, i.e. $dz = dz(d\mathbf{x})$, is:

$$dz = \lim_{\epsilon\to 0}\frac{z(\mathbf{x}+\epsilon\,\Delta\mathbf{x}) - z(\mathbf{x})}{\epsilon} = \left.\frac{\partial z(\mathbf{x}+\epsilon\,\Delta\mathbf{x})}{\partial\epsilon}\right|_{\epsilon=0} \tag{70}$$

Consequently, to construct a *consistent* tangent matrix for our problem, we start with the discrete version of the equations, substitute for any variable the incremented ones:

$$\mathbf{s} \to \mathbf{s}_\epsilon = \mathbf{s} + \epsilon\,\Delta\mathbf{s}\,, \quad \mathbf{e} \to \mathbf{e}_\epsilon = \mathbf{e} + \epsilon\,\Delta\mathbf{e}$$

$$\mathbf{n} \to \mathbf{n}_\epsilon = \mathbf{n} + \epsilon\,\Delta\mathbf{n}\,, \quad \lambda \to \lambda_\epsilon = \lambda + \epsilon\,\Delta\lambda \tag{71}$$

and compute the derivative with respect to ϵ at $\epsilon = 0$.

Linearizing the equations:

$$\mathbf{s} = 2G(\mathbf{e} - \mathbf{e}_n^p) - 2G\,\lambda\,\mathbf{n} \tag{72}$$

$$\boldsymbol{\alpha} = \boldsymbol{\alpha}_n + \frac{2}{3}H_{kin}\,\lambda\,\mathbf{n} \tag{73}$$

about a solution point, we get:

$$d\mathbf{s} = 2Gd\mathbf{e} - 2G\mathbf{n}d\lambda - 2G\lambda d\mathbf{n} \tag{74}$$

$$d\boldsymbol{\alpha} = \frac{2}{3}H_{kin}\mathbf{n}d\lambda + \frac{2}{3}H_{kin}\lambda d\mathbf{n} \tag{75}$$

Using the relation:

$$d\mathbf{n} = \frac{1}{\|\boldsymbol{\Sigma}\|}\ [\mathbf{I} - \mathbf{n} \otimes \mathbf{n}]\ (d\mathbf{s} - d\boldsymbol{\alpha}) \tag{76}$$

derived in Appendix 1, equations (74) and (75) can be rewritten as:

$$\left[\mathbf{I} + a\hat{\mathbf{I}}\right] d\mathbf{s} = 2Gd\mathbf{e} - 2G\mathbf{n}d\lambda + a\hat{\mathbf{I}}d\boldsymbol{\alpha} \tag{77}$$

$$\left[\mathbf{I} + b\hat{\mathbf{I}}\right] d\boldsymbol{\alpha} = b\hat{\mathbf{I}}d\mathbf{s} + \frac{2}{3}H_{kin}\mathbf{n}d\lambda \tag{78}$$

where:

$$\hat{\mathbf{I}} = [\mathbf{I} - (\mathbf{n} \otimes \mathbf{n})]\ ,\ \ a = \frac{2G\lambda}{\|\boldsymbol{\Sigma}\|}\ ,\ \ b = \frac{2}{3}\frac{H_{kin}\lambda}{\|\boldsymbol{\Sigma}\|} \tag{79}$$

and $\mathbf{I}$ is the fourth order identity tensor. Equations (77) and (78) can now be recast in a matrix form in terms of the unknown $d\mathbf{s}$, $d\boldsymbol{\alpha}$, $d\lambda$:

$$\begin{bmatrix} \mathbf{I} + a\hat{\mathbf{I}} & -a\hat{\mathbf{I}} & 2G\mathbf{n} \\ -b\hat{\mathbf{I}} & \mathbf{I} + b\hat{\mathbf{I}} & -\frac{2}{3}H_{kin}\mathbf{n} \end{bmatrix} \begin{Bmatrix} d\mathbf{s} \\ d\boldsymbol{\alpha} \\ d\lambda \end{Bmatrix} = \begin{Bmatrix} 2Gd\mathbf{e} \\ \mathbf{0} \end{Bmatrix} \tag{80}$$

As shown in the next section, the linearization of the limit equation for all the models discussed in Section 4 can be expressed in the form:

$$d\lambda = A\,(\mathbf{n} : d\mathbf{e}) \tag{81}$$

Inserting equation (81) into equation (80) yields:

$$\mathbf{A}\mathbf{x} = \mathbf{y} \tag{82}$$

where:

$$\mathbf{A} = \begin{bmatrix} \mathbf{I} + a\hat{\mathbf{I}} & -a\hat{\mathbf{I}} \\ -b\hat{\mathbf{I}} & \mathbf{I} + b\hat{\mathbf{I}} \end{bmatrix} \tag{83}$$

$$\mathbf{x} = \begin{Bmatrix} d\mathbf{s} \\ d\boldsymbol{\alpha} \end{Bmatrix} \tag{84}$$

$$\mathbf{y} = \begin{Bmatrix} 2G\,[\mathbf{I} - A(\mathbf{n} \otimes \mathbf{n})]\,d\mathbf{e} \\ \frac{2}{3}H_{kin}(\mathbf{n} \otimes \mathbf{n})d\mathbf{e} \end{Bmatrix} = \begin{Bmatrix} 2G\left[(1+A)\mathbf{I} - A\hat{\mathbf{I}}\right] d\mathbf{e} \\ \frac{2}{3}H_{kin}(\mathbf{n} \otimes \mathbf{n})d\mathbf{e} \end{Bmatrix} \tag{85}$$

To solve the system, we assume a generalization of the Sherman-Morrison formula for the inverse of the matrix $\mathbf{A}$, in the form:

$$\mathbf{A}^{-1} = \begin{bmatrix} \mathbf{I} - C\hat{\mathbf{I}} & -E\hat{\mathbf{I}} \\ -F\hat{\mathbf{I}} & \mathbf{I} - D\hat{\mathbf{I}} \end{bmatrix} \tag{86}$$

and, requiring that $\mathbf{A}\mathbf{A}^{-1} = \mathbf{I}$, the four unknowns C, E, F, D can be computed. As shown in Appendix 2, the result is:

$$C = E = \frac{a}{1 + a + b} = \frac{2G\lambda}{\|\boldsymbol{\Sigma}^{TR}\|} \tag{87}$$

$$D = F = \frac{b}{1+a+b} = \frac{2}{3}\frac{\lambda H_{kin}}{\|\boldsymbol{\Sigma}^{TR}\|} \tag{88}$$

such that the solution of (82) can be rewritten in an explicit form:

$$\left\{ \begin{array}{c} d\mathbf{s} \\ d\boldsymbol{\alpha} \end{array} \right\} = \left[\begin{array}{cc} \mathbf{I} - C\hat{\mathbf{I}} & -C\hat{\mathbf{I}} \\ -D\hat{\mathbf{I}} & \mathbf{I} - D\hat{\mathbf{I}} \end{array} \right] \left\{ \begin{array}{c} 2G\left[(1+A)\mathbf{I} - A\hat{\mathbf{I}}\right] d\mathbf{e} \\ \frac{2}{3}H_{kin}(\mathbf{n}\otimes\mathbf{n})d\mathbf{e} \end{array} \right\} \tag{89}$$

which, upon expansion of the first row, yields the relation:

$$d\mathbf{s} = 2G\left[(1-C)\mathbf{I} + (C-A)\left(\mathbf{n}\otimes\mathbf{n}\right)\right] d\mathbf{e} \tag{90}$$

This is a consistent incremental relation between the deviatoric part of the stress tensor $\mathbf{s}$ and the deviatoric part of the strain tensor $\mathbf{e}$; however, our final goal is to obtain an incremental relation between the total stress tensor $\boldsymbol{\sigma}$ and the total strain tensor $\boldsymbol{\epsilon}$. Therefore, in equation (90) first of all we have to express $\mathbf{e}$ in terms of $\boldsymbol{\epsilon}$, secondly we need to include the volumetric part of the stress tensor. The first step can be easily performed since:

$$d\mathbf{e} = \mathbf{I}_{dev} d\boldsymbol{\epsilon} \tag{91}$$

where $\mathbf{I}_{dev}$ is a rank four tensor able to filter only the deviatoric part from any generic second order tensor and is given by:

$$\mathbf{I}_{dev} = \mathbf{I} - \frac{1}{3}(\mathbf{1}\otimes\mathbf{1}) \tag{92}$$

Using (91), equation (90) can be rewritten as:

$$d\mathbf{s} = 2G\left[(1-p)\mathbf{I}_{dev} + (p-A)\left(\mathbf{n}\otimes\mathbf{n}\right)\right] d\boldsymbol{\epsilon} \tag{93}$$

In order to take into account the volumetric portion of the stress tensor, we recall that:

$$\boldsymbol{\sigma} = p\,\mathbf{1} + \mathbf{s} \tag{94}$$

where, assuming linear elasticity:

$$p = \frac{1}{3}\left(\mathbf{1} : \boldsymbol{\sigma}\right) = K\,\mathrm{tr}(\boldsymbol{\epsilon}) = K\left(\mathbf{1} : \boldsymbol{\epsilon}\right) \tag{95}$$

with p the pressure and K the bulk modulus. From (95) we deduce that:

$$p\,\mathbf{1} = K(\mathbf{1}\otimes\mathbf{1})\,\boldsymbol{\epsilon} \tag{96}$$

since $(\mathbf{1}\otimes\mathbf{1})$ is the counterpart of $\mathbf{I}_{dev}$ for the volumetric part, i.e. is the rank four tensor able to filter only the volumetric part from any second order tensor. Using the incremental version of (96) in (93), we get the final expression which we seek:

$$d\boldsymbol{\sigma} = \mathbf{D}^{ep} d\boldsymbol{\epsilon} \tag{97}$$

where the algorithmic elastic-inelastic tangent tensor is given by:

$$\mathbf{D}^{ep} = \left[K\left(\mathbf{1}\otimes\mathbf{1}\right) + 2G\left(1-C\right)\mathbf{I}_{dev} + 2G\left(C-A\right)\left(\mathbf{n}\otimes\mathbf{n}\right)\right] \tag{98}$$

We recall that:

$$C = \frac{2G\lambda}{\|\boldsymbol{\Sigma}^{TR}\|} = \frac{2G\lambda}{\|\boldsymbol{\Sigma}\| + \left(2G + \frac{2}{3}H_{kin}\lambda\right)} \tag{99}$$

and A comes from a specific linearized material model.

It is interesting to point out that not only a straightforward approach for the construction of the consistent tangent matrix has been shown but also that, for any material model for which we can assume a linearized yield equation of the form $d\lambda = A\,(\mathbf{n} \cdot d\mathbf{e})$, we obtain a symmetric tangent matrix.

6. Consistent tangent moduli for plasticity and visco-plasticity models

In Section 5 we computed the general expression for the tangent matrix, consistent with the discrete equations introduced in Section 3. The form proposed involves a coefficient A coming from the linearization of the discrete form of the appropriate limit equation. In the following we show how it is possible to particularize this scalar factor for the material models considered in Section 4.

6.1. Classical plasticity

For the classical plasticity model, the discrete limit equation is:

$$dg = df = d\|\boldsymbol{\Sigma}\| - dR = d\|\boldsymbol{\Sigma}\| - \frac{2}{3}H_{iso}d\lambda = 0 \tag{100}$$

Since $d\|\boldsymbol{\Sigma}\| = \mathbf{n} : (d\mathbf{s} - d\boldsymbol{\alpha})$, as deduced in Appendix 1, we can rewrite equation (100):

$$(\mathbf{n} : d\mathbf{s}) - (\mathbf{n} : d\boldsymbol{\alpha}) - \frac{2}{3}H_{iso}\, d\lambda = 0 \tag{101}$$

Recalling equations (74) and (75) and that:

$$d\mathbf{n} = \frac{1}{\|\boldsymbol{\Sigma}\|}\hat{\mathbf{I}}\, d\boldsymbol{\Sigma} \quad , \qquad \hat{\mathbf{I}}\mathbf{n} = \mathbf{0} \tag{102}$$

as derived in Appendix 2, we get:

$$df = 2G\,(\mathbf{n} : d\mathbf{e}) - 2G_1 d\lambda = 0 \tag{103}$$

Solving for $d\lambda$, we end up with:

$$d\lambda = A(\mathbf{n} : d\mathbf{e}) \tag{104}$$

where:

$$A = \frac{G}{G_1} \tag{105}$$

6.2. Classical visco-plasticity

For the classical visco-plasticity model, the discrete limit equation is:

$$\left(\frac{f}{R_0}\right)^m \Delta t - \frac{\eta}{R_0}\lambda = 0 \tag{106}$$

The corresponding linearized form is:

$$m\Delta t \left(\frac{f}{R_0}\right)^{m-1} df - \eta d\lambda = 0 \tag{107}$$

Inserting (103) in the above, we get:

$$[2G(\mathbf{n} : d\mathbf{e}) - 2G_1 d\lambda] - C_1 \eta d\lambda = 0 \tag{108}$$

where:

$$C_1 = \frac{1}{m\Delta t}\left(\frac{f}{R_0}\right)^{m-1} \tag{109}$$

Solving for $d\lambda$, we obtain:

$$d\lambda = A\,(\mathbf{n} : d\mathbf{e}) \tag{110}$$

with:

$$A = \frac{2G}{C_1\eta + 2G_1} \tag{111}$$

For $\eta \to 0$, we recover the classical plasticity tangent parameter.

6.3. Generalized plasticity

The discrete version of the limit equation for this model is equation (55), and, upon clearing fractions, becomes:

$$\left[\zeta(r - f) + \frac{2}{3}Hr\right]\lambda = f\left[\|\boldsymbol{\Sigma}\| - \|\boldsymbol{\Sigma}_n\| + \frac{2}{3}H_{kin}\lambda\right] \tag{112}$$

Linearizing and again using the expression for df and $d\|\boldsymbol{\Sigma}\|$, we get:

$$d\lambda = A\,(\mathbf{n} : d\mathbf{e}) \tag{113}$$

where:

$$A = \frac{2G(B_1 + B_2)}{2G_1 B_1 + (2G - \zeta)B_2 + B_3} \tag{114}$$

with:

$$\begin{aligned} B_1 &= \|\boldsymbol{\Sigma}\| - \|\boldsymbol{\Sigma}_n\| + \left(\frac{2}{3}H_{kin} + \zeta\right)\lambda \\ B_2 &= f = \|\boldsymbol{\Sigma}\| - \left(R_n + \frac{2}{3}H_{iso}\lambda\right) \\ B_3 &= \left(\zeta + \frac{2}{3}H\right)r \end{aligned} \tag{115}$$

Note that if $r = 0$ then $B_2 = B_3 = 0$ and we end up with the tangent matrix of the classical plasticity model.

6.4. Generalized visco-plasticity

The discrete version of the limit equation for this model is equation (67), that can be rewritten as:

$$\left[\zeta(r-f)+\frac{2}{3}Hr\right]\lambda - f\left[\|\boldsymbol{\Sigma}\| - \|\boldsymbol{\Sigma}_n\| + \frac{2}{3}H_{kin}\lambda\right] - \left[\zeta(r-f)+\frac{2}{3}Hr\right]f\frac{\Delta t}{\eta} = 0 \quad (116)$$

Linearizing and again using the expression for df and $d\|\boldsymbol{\Sigma}\|$, we get:

$$d\lambda = A\,(\mathbf{n} : d\mathbf{e}) \quad (117)$$

with:

$$A = \frac{2G(B_1+B_2+B_4)}{2G_1B_1+(2G-\zeta)B_2+B_3+2G_2B_4} \quad (118)$$

where B_1 , B_2 and B_3 have already been defined in Section 6.3 and:

$$B_4 = \frac{\Delta t}{\eta}(B_3 - 2\zeta B_2) \quad , \quad G_2 = G + \frac{1}{3}H_{iso} \quad (119)$$

For $\eta \to \infty$, we recover the tangent matrix parameter for the generalized plasticity model.

7. Numerical examples

In this section we present several numerical simulations to test the performance and the behavior of some of the models previously discussed. Since this is the first time in which the generalized models are tested within a finite element setting, we prefer to concentrate and limit our computations to the rate-independent models, i.e. classical plasticity and generalized plasticity. All the numerical example described are obtained running a three dimensional isoparametric element, which uses a *mixed B-bar* approach for the construction of the tangent matrix [19]. The element is implemented into the Finite Element Analysis Program (FEAP) [20, 21].

The numerical simulations are organized as follow:

- Uniaxial test: loading-unloading
- Uniaxial test: cyclic load
- Thick walled tube under internal pressure
- Thin walled tube in tension and torsion: displacement control
- Thin walled tube in tension and torsion: force control

7.1. Uniaxial test: loading-unloading

In this example we consider a cubic specimen of side length equal to 10 with boundary condition and loading set to produce a stress state of uniaxial tension. The sample is modeled with only one element and the material properties are:

$$E = 100\ , \quad \nu = 0.3\ , \quad \sigma_y = 10 \tag{120}$$

$$\beta \in \{0, 3\}\ , \quad \frac{\delta}{2G} \in \left\{0, \frac{1}{2}, 1, 10\right\}\ , \quad H \in \{-5, 0, 5\} \tag{121}$$

First we present some basic results to show the general performance of the generalized model. In fig.1, $\beta = 3, \delta = G$ and $H = 0$. The solution obtained from the generalized model is compared with the one obtained from the classical model. Note that the generalized model performs as expected. That is:

- it shows a soft curvature before reaching the asymptote,
- if unloaded from the plastic range, upon reloading, it shows renewed plasticity before the attainment of the stress where unloading began.

In fig.2, the hardening parameter is varied using the prescribed set of values. It is interesting to note that the generalized model allows one to use negative values of the hardening parameters and, therefore, is able to model materials with softening behavior.

In figs.3 to 7, the influence of the different parameters involved in the analysis is considered. From these results some observations may be made:

- The asymptote is approached faster for larger values of δ and, as a matter of fact, this parameter measures the speed of the model toward the limiting behavior (fig.3).
- the model always approaches the correct limit that for the case of a uniaxial tension test is:

$$\sigma(t \to \infty) = \sigma_y + \beta + H\epsilon^p \tag{122}$$

  (figs.1, 6, 7).
- The generalized model always reduces to the classical one for $\beta = 0$ (figs.4 and 5).
- For $\delta = 0$ we get the classical solution independently from the β value if $H = 0$; we do not get the classical solution if $H \neq 0$ (figs.3 and 6). This agrees with the theoretical results shown in Section 5.3.
- The generalized model retains its properties also for negative values of H with $\beta > 0$ (fig.7).

7.2. Uniaxial test: cyclic load

In this example we consider again a cubic specimen with side length equal to 10. This time the sample undergoes a cyclic uniaxial load history (fig.8). The material properties are:

$$E = 100, \quad \nu = 0.3 \quad \sigma_y = 10 \tag{123}$$

while $H_{kin} \in \{10, -5\}$ with $\beta = 3$, $\delta = G$, $H_{iso} = 0$. The axial stress is plotted versus the axial strain in figs.9 and 10. For the case $H_{kin} = 10$ the solution of the classical model is also reported in fig.11 for comparison purposes. Observe that the model retains all its properties also in the case of cyclic loads, showing them in each cycle.

7.3. Thick walled tube under pressure

We next consider a long thick walled cylinder subjected to an internal pressure loading. The inner and the outer radii of the cylinder are 2 and 10, respectively. The material properties are:

$$E = 10^6 \ , \quad \nu = 0.3 \ , \quad \sigma_y = 1000 \tag{124}$$

while:

$$\delta = 1000 \ , \quad \beta = 500 \ , \quad H = 0 \tag{125}$$

We simulate the internal pressure effects by controlling the inner displacement and, as a result, the applied load history is expressed in terms of this quantity. The displacement is increased linearly in time from 0 at time 0 to 20 at time 10, and then it is linearly decreased to reach the value 0 at time 20. The radial stress at the inner radius is computed and reported versus time in fig.12. The solution from the classical plasticity model ($\beta = 0$) is also presented for comparison.

7.4. Thin walled tube in tension and torsion: displacement control

We consider a thin walled circular tube; the inner and the outer radii are 9.75 and 10.25, respectively. The material properties are:

$$E = 300 \ , \quad \nu = 0.3 \ , \quad \sigma_y = 10 \tag{126}$$

and:

$$\delta = 30, \quad \beta = 5 \ , \quad H = 0 \tag{127}$$

The tube is loaded by controlling the displacements. The load history - in terms of the strains - is represented in figs.13 and 14: the tube is initially pulled in tension, beyond the yielding limit, and then a tangential displacement (torsion) is applied, leaving the axial displacement unchanged. The axial and the tangential stresses are plotted versus time in figs.15 and 16. It is interesting to note that, as the shear stress approaches the limiting value, the axial stress approaches zero and a virtually pure torsion is attained. Hence the elastic part of the constant axial strain changes from purely elastic to plastic, as the tangential displacement is increased. This behavior can be proved to be correct in closed form for the classical model [1] and here is obtained computationally for both the models. In fig.17 a three dimensional mesh used for this problem is shown.

7.5. Thin walled tube in tension and torsion: force control

Finally, we consider the tube described in the previous test, loaded under stress control. The material properties are:

$$E = 13000 \ , \quad \nu = 0.3 \ , \quad \sigma_y = 16 \tag{128}$$

and:

$$\delta = 2000 \ , \quad \beta = 16 \ , \quad H = 600 \tag{129}$$

The tube is stretched until a certain value $\bar{\sigma}$ of axial stress and then, leaving this quantity unchanged, a torque is applied. An analytical solution for the generalized model is available [18] for the different values of $\bar{\sigma}$. In figs.18, 19 and 20 the numerical and the analytical

solutions are reported, for $\bar{\sigma} \in \{0, 16, 32\}$: the solutions match perfectly. In fig.21 the tangential stress $\sigma_{z\theta}$ is plotted versus the tangential strain $\gamma_{z\theta}$ for three different values of $\bar{\sigma}$:

$$\bar{\sigma} \in \{0, 16, 32\} \tag{130}$$

8. Closure

In this work we review the application of a return mapping algorithm to classical plasticity and visco-plasticity. In addition, we extend its application to include the generalized plasticity and visco-plasticity models introduced in References 18. The implementation of all these models fits within the simple integration radial return algorithm adopted here.

For applications using the finite element method and a Newton solution technique, we also include a development of the consistent algorithmic tangent matrix for all the material models. The development includes both isotropic and kinematic hardening.

Solution of some example problems using the generalized models show some interesting features such as: they *smoothly* reach a limiting asymptote for both monotonic and cyclic loading conditions; if unloaded in the plastic range, upon reloading, they show renewed plasticity before the attainment of the stress where unloading began.

Finally, we note that the classical visco-plasticity model and the generalized plasticity and visco-plasticity models may be implemented into existing finite element programs, originally limited to plasticity alone, with only minor modification and extension. Namely, the current limit equation and its appropriate tangent factors A and C appearing in equation (98) must be specialized for each model.

Appendix n.1

In this appendix we show that the following equalities hold:

$$d\mathbf{n} = \frac{1}{\|\boldsymbol{\Sigma}\|}\hat{\mathbf{I}}\, d\boldsymbol{\Sigma} = \frac{1}{\|\boldsymbol{\Sigma}\|}\left[\mathbf{I} - \mathbf{n}\otimes\mathbf{n}\right]\left(\, d\mathbf{s} - \, d\boldsymbol{\alpha}\right) \tag{131}$$

Using the definition of the tangent value as in Section 4, we can write:

$$d\mathbf{n} = \frac{\partial}{\partial\epsilon}\left(\mathbf{n}_\epsilon\right)\Big|_{\epsilon=0} = \frac{\partial}{\partial\epsilon}\left(\frac{\boldsymbol{\Sigma}_\epsilon}{\|\boldsymbol{\Sigma}_\epsilon\|}\right)\Big|_{\epsilon=0} \tag{132}$$

but:

$$\begin{aligned} d\|\boldsymbol{\Sigma}\| &= \frac{\partial}{\partial\epsilon}\left(\|\boldsymbol{\Sigma}_\epsilon\|\right)\Big|_{\epsilon=0} = \frac{\partial}{\partial\epsilon}\left[\left(\boldsymbol{\Sigma}_\epsilon : \boldsymbol{\Sigma}_\epsilon\right)^{1/2}\right]\Big|_{\epsilon=0} = \\ &= \left[\frac{1}{\|\boldsymbol{\Sigma}_\epsilon\|}\boldsymbol{\Sigma}_\epsilon : d\boldsymbol{\Sigma}\right]\Big|_{\epsilon=0} = \\ &= \left[\frac{1}{\|\boldsymbol{\Sigma}\|}\boldsymbol{\Sigma} : d\boldsymbol{\Sigma}\right] = \mathbf{n} : d\boldsymbol{\Sigma} \end{aligned} \tag{133}$$

So:

$$\begin{aligned} d\mathbf{n} &= \frac{1}{\|\boldsymbol{\Sigma}\|^2}\left[\frac{\partial}{\partial\epsilon}\boldsymbol{\Sigma}_\epsilon\|\boldsymbol{\Sigma}_\epsilon\| - \boldsymbol{\Sigma}_\epsilon\frac{\partial}{\partial\epsilon}\|\boldsymbol{\Sigma}_\epsilon\|\right]\Big|_{\epsilon=0} \\ &= \frac{1}{\|\boldsymbol{\Sigma}\|^2}\left[d\boldsymbol{\Sigma}\|\boldsymbol{\Sigma}\| - \boldsymbol{\Sigma}(\mathbf{n} : d\boldsymbol{\Sigma})\right] = \frac{1}{\|\boldsymbol{\Sigma}\|}\left[d\boldsymbol{\Sigma} - (\mathbf{n}\otimes\mathbf{n})d\boldsymbol{\Sigma}\right] \\ &= \frac{1}{\|\boldsymbol{\Sigma}\|}\left[\mathbf{I} - (\mathbf{n}\otimes\mathbf{n})\right]\, d\boldsymbol{\Sigma} = \frac{1}{\|\boldsymbol{\Sigma}\|}\hat{\mathbf{I}}\, d\boldsymbol{\Sigma} \end{aligned} \tag{134}$$

Appendix n.2

In this appendix we show some properties of the tensor $\hat{\mathbf{I}}$ and a way to construct the inverse of the matrix $\mathbf{A}$, introduced and used in Section 4.

The first useful property of $\hat{\mathbf{I}}$ is:

$$\hat{\mathbf{I}}\mathbf{n} = \mathbf{0} \tag{135}$$

In fact:

$$\hat{\mathbf{I}}\mathbf{n} = \left[\mathbf{I} - (\mathbf{n}\otimes\mathbf{n})\right]\mathbf{n} = \mathbf{n} - (\mathbf{n}\otimes\mathbf{n})\mathbf{n} = \mathbf{n} - \mathbf{n} = \mathbf{0} \tag{136}$$

The other property is:

$$\hat{\mathbf{I}}^n = \hat{\mathbf{I}} \tag{137}$$

for any integer n. We can prove that the relation holds for $n = 2$ and then for any value of n the proof comes by induction. We have:

$$\begin{aligned} \hat{\mathbf{I}}^2 &= \left[\mathbf{I} - (\mathbf{n}\otimes\mathbf{n})\right]\left[\mathbf{I} - (\mathbf{n}\otimes\mathbf{n})\right] \\ &= \mathbf{I} - 2(\mathbf{n}\otimes\mathbf{n}) + (\mathbf{n}\otimes\mathbf{n})(\mathbf{n}\otimes\mathbf{n}) \\ &= \mathbf{I} - 2(\mathbf{n}\otimes\mathbf{n}) + (\mathbf{n}\otimes\mathbf{n}) = \mathbf{I} - (\mathbf{n}\otimes\mathbf{n}) \end{aligned} \tag{138}$$

At this point we can look at the construction of the inverse of matrix $\mathbf{A}$, where:

$$\mathbf{A} = \begin{bmatrix} \mathbf{I} + a\hat{\mathbf{I}} & -a\hat{\mathbf{I}} \\ -b\hat{\mathbf{I}} & \mathbf{I} + b\hat{\mathbf{I}} \end{bmatrix} \tag{139}$$

Due to the particular form of $\mathbf{A}$, we assume a similar form also for its inverse (suggested by the Sherman-Morrison formula):

$$\mathbf{A}^{-1} = \begin{bmatrix} \mathbf{I} - C\hat{\mathbf{I}} & -E\hat{\mathbf{I}} \\ -F\hat{\mathbf{I}} & \mathbf{I} - D\hat{\mathbf{I}} \end{bmatrix} \tag{140}$$

Requiring that $\mathbf{A}\mathbf{A}^{-1} = \mathbf{I}$, we obtain a system of four sets of equations in the four unknowns C, D, E, F. Simplifying the equations, we end up with the following system:

$$\begin{aligned} \mathbf{I}+ \quad (a - C - aC + aF)\hat{\mathbf{I}} &= \mathbf{I} \\ (-b + bC - F - bF)\hat{\mathbf{I}} &= \mathbf{0} \\ (-E - aE - a + aD)\hat{\mathbf{I}} &= \mathbf{0} \\ \mathbf{I}+ \quad (bE + b - D - bD)\hat{\mathbf{I}} &= \mathbf{I} \end{aligned} \tag{141}$$

A solution results when the coefficient of the $\hat{\mathbf{I}}$ tensor are zero. We obtain a system of four equations in the four unknowns, which can be decoupled into two smaller systems, each of only two scalar equations. The solution is:

$$C = E = \frac{a}{1 + a + b} = \frac{2G\lambda}{\|\boldsymbol{\Sigma}^{TR}\|} \tag{142}$$

$$D = F = \frac{b}{1 + a + b} = \frac{2}{3}\frac{\lambda H_{kin}}{\|\boldsymbol{\Sigma}^{TR}\|} \tag{143}$$

Substituting these values back in (140), we get:

$$\mathbf{A}^{-1} = \begin{bmatrix} \mathbf{I} - C\hat{\mathbf{I}} & -C\hat{\mathbf{I}} \\ -D\hat{\mathbf{I}} & \mathbf{I} - D\hat{\mathbf{I}} \end{bmatrix} \tag{144}$$

which is the matrix used in Section 5.

References

[1] J.Lubliner, *Plasticity theory*, Macmillan, 1990

[2] W.F.Chen and D.J.Han, *Plasticity for structural engineers*, Springer-Verlag, 1988

[3] G.Maenchen and S.Sack, "The tensor code", Methods in computational physics, ed. B.Alder, **3**, pp. 181-210, 1964, Academic Press

[4] M.L.Wilkins, "Calculation of elastic plastic flow", Methods in computational physics, ed. B.Alder, **3**, pp. 211-263, 1964, Academic Press

[5] G.Dahlquist and $\mathring{A}$.Björck, *Numerical methods*, Prentice-Hall Inc, 1974

[6] Gear C.W., *Numerical initial value problems in ordinary differential equations*, Prentice Hall, Englewood Cliff, 1971

[7] J.C.Nagtegaal, "On the implementation of inelastic constitutive equations with special reference to large deformation problems", Computer Methods in Applied Mechanics and Engineering, **33**, pp. 469-484, 1982

[8] J.C.Simo and R.L.Taylor, "Consistent tangent operators for rate-independent elastoplasticity", Computer Methods in Applied Mechanics and Engineering, **48**, pp. 101-118, 1985

[9] M.Ortiz and J.C.Simo, "An analysis of a new class of integration algorithms for elastoplastic constitutive relations", International Journal for Numerical Methods in Engineering **23**, pp. 353-366, 1986

[10] R.D.Krieg and D.B.Krieg, "Accuracies of numerical solution methods for the elastic-perfectly plastic model", Journal of Pressure Vessel Technology, Transaction of ASME, pp. 510-515, November 1977

[11] M.Ortiz and E.P.Popov, "Accuracy and stability of integration algorithms for elastoplastic constitutive relations", International Journal for Numerical Methods in Engineering **21**, pp. 1561-1576, 1985

[12] J.C.Simo and S.Govindjee, "Non-linear B-stability and symmetry preserving return mapping algorithms for plasticity and viscoplasticity", International Journal for Numerical Methods in Engineering **31**, pp. 151-176, 1991

[13] J.C.Simo and R.L.Taylor, "A return mapping algorithm for plane stress elastoplasticity", International Journal for Numerical Methods in Engineering **22**, pp. 649-670, 1986

[14] J.C.Simo, J.G.Kennedy and S.Govindjee, "Non-smooth multisurface plasticity and viscoplasticity. Loading/unloading conditions and numerical algorithms", International Journal for Numerical Methods in Engineering **26**, pp. 2161-2185, 1988

[15] J.C.Simo and T.J.R.Hughes, *Elasto-plasticity and viscoplasticity: computational aspects*, Springer-Verlag, to appear

[16] P.Perzyna, "The constitutive equations for rate sensitive plastic materials", Q.Appl.Math., **20**, n.4, pp. 321-332, 1963

[17] J.Lubliner, "A simple model of generalized plasticity", Int.J.Solids Structures, **28**, n.6, pp. 769-779, 1991

[18] J.Lubliner, R.L.Taylor and F.Auricchio, "Generalized plasticity and visco-plasticity", *to appear*

[19] J.C.Simo, R.L.Taylor and K.S.Pister, "Variational and projection methods for the volume constraint in finite deformation elasto-plasticity", Computer Methods in Applied Mechanics and Engineering, **51**, pp. 177-208, 1985

[20] O.C.Zienkiewicz and R.L.Taylor, *The finite element method*, McGraw Hill, New York, 4th ed., 1989, vol. I

[21] O.C.Zienkiewicz and R.L.Taylor, *The finite element method*, McGraw Hill, New York, 4th ed., 1991, vol. II

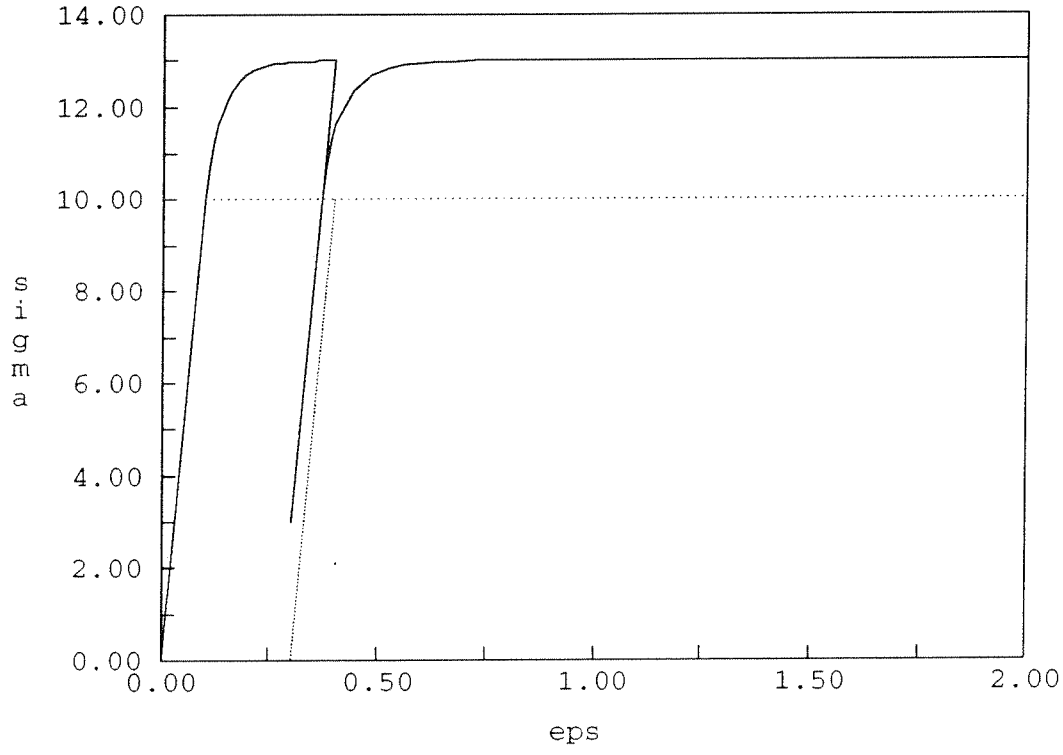

Figure 1: Uniaxial test: loading-unloading. $\beta = 3$, $\delta = G$, $H = 0$. For comparison, the solution from the classical model is also presented with a dotted line.

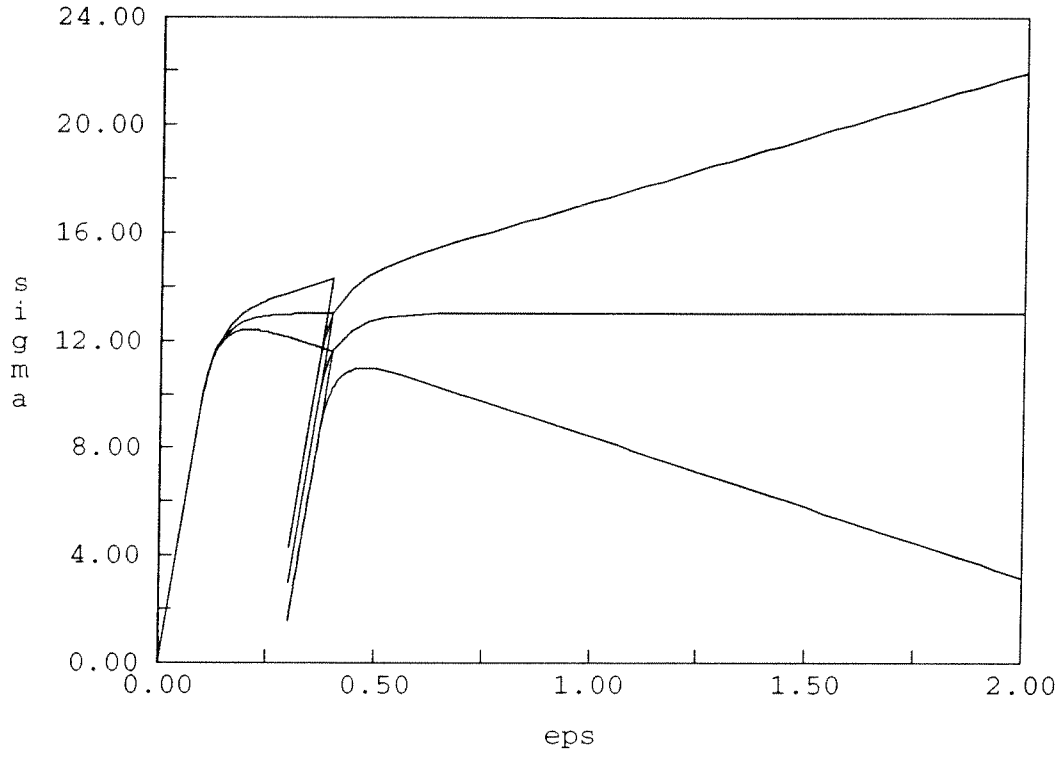

Figure 2: Uniaxial test: loading-unloading. $\beta = 3$, $\delta = G$, $H \in \{-5, 0, 5\}$

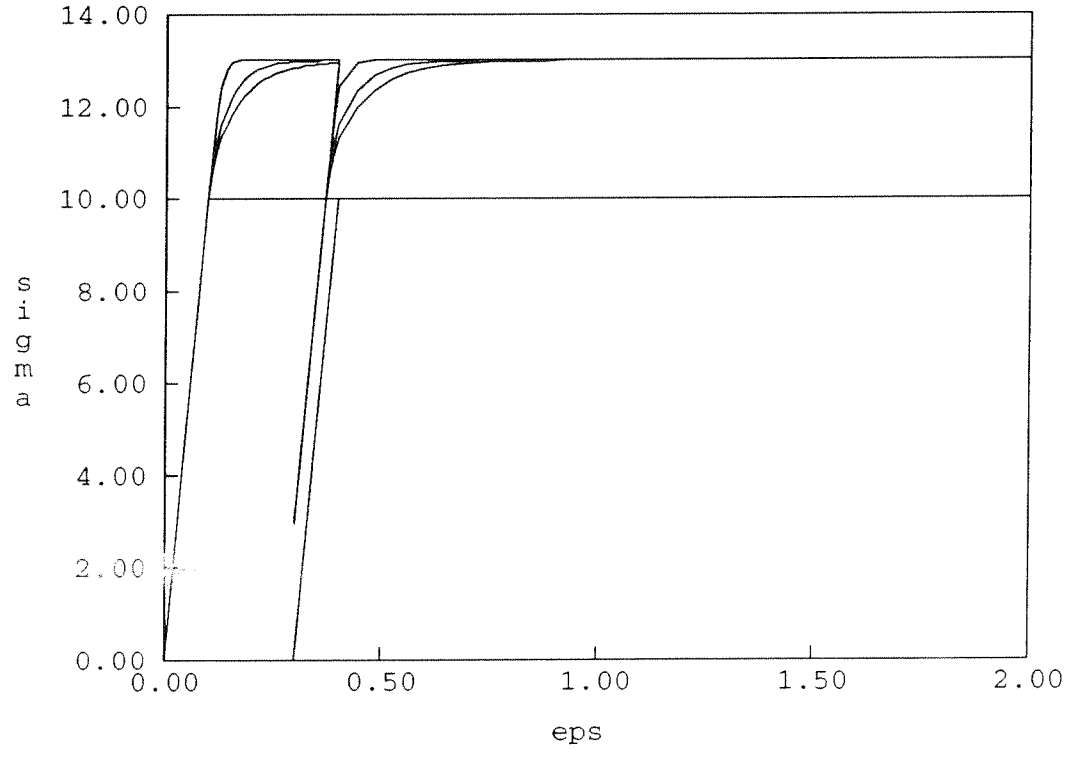

Figure 3: Uniaxial test: loading-unloading. $\beta = 3, \delta/2G \in \{0, \frac{1}{2}, 1, 10\}, H = 0$

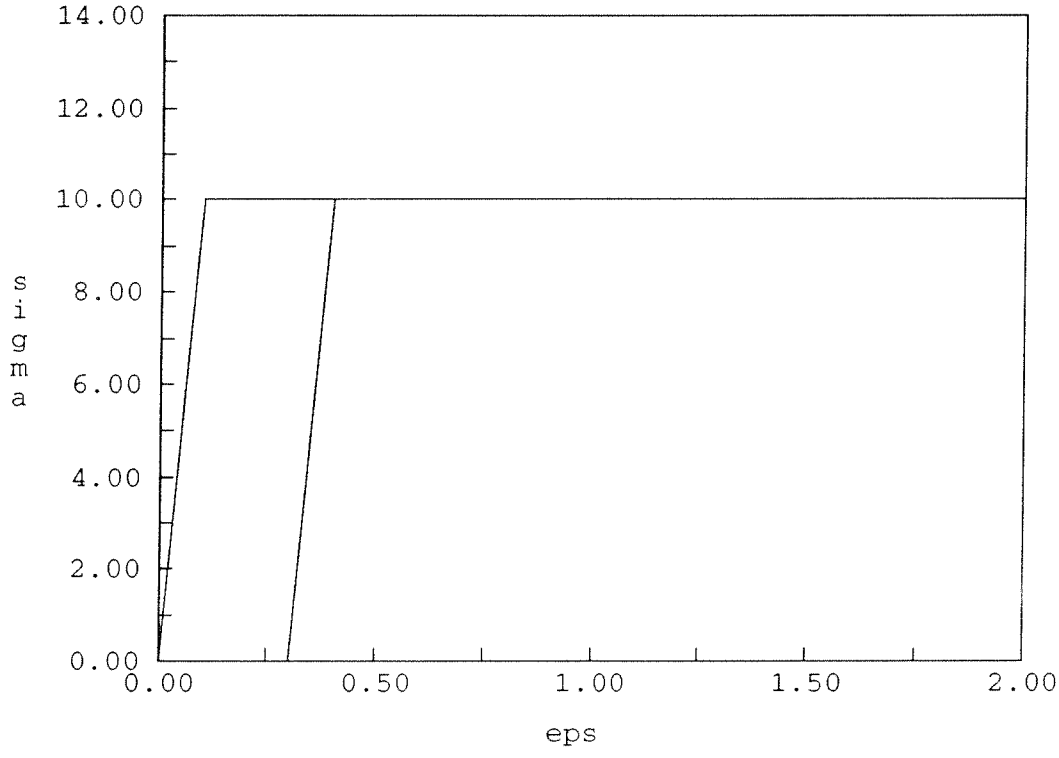

Figure 4: Uniaxial test: loading-unloading. $\beta = 0, \delta/2G \in \{0, \frac{1}{2}, 1, 10\}, H = 0$

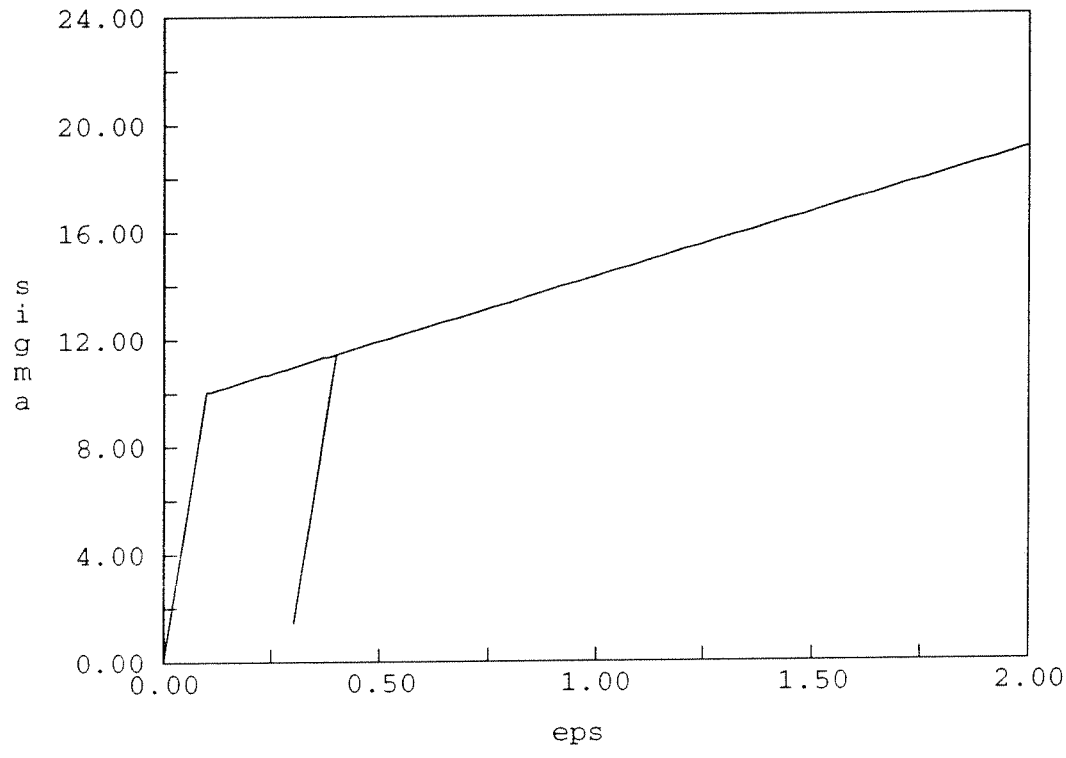

Figure 5: Uniaxial test: loading-unloading. $\beta = 0, \delta/2G \in \{0, \frac{1}{2}, 1, 10\}, H = 5$

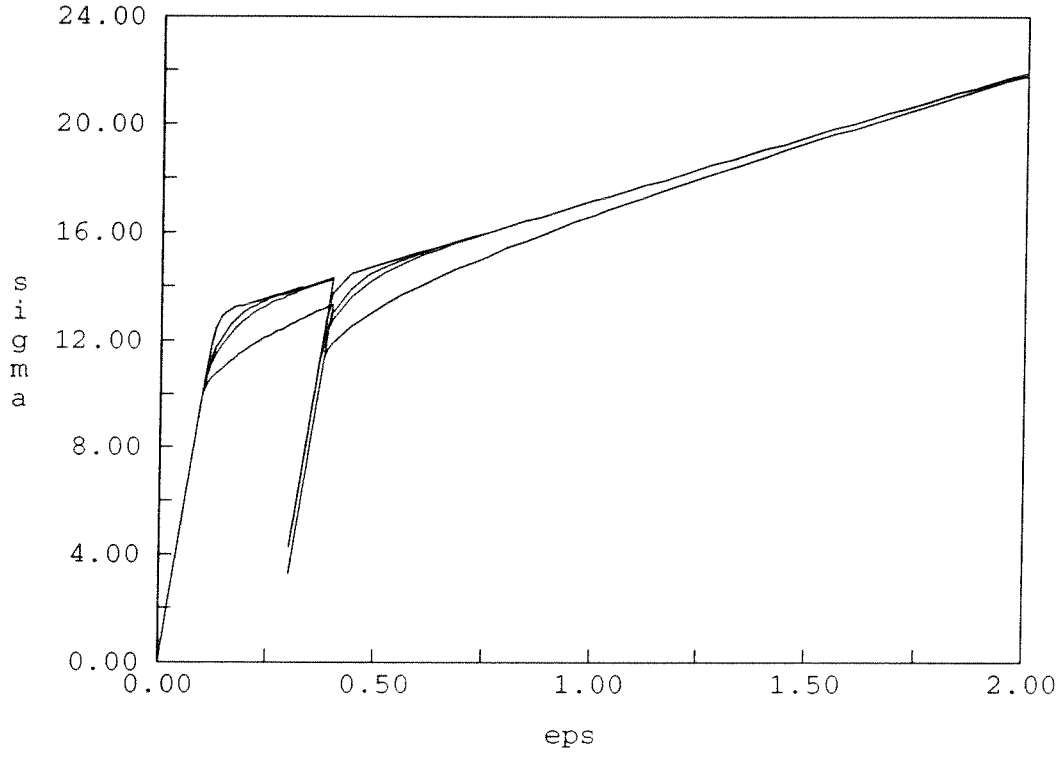

Figure 6: Uniaxial test: loading-unloading. $\beta = 3, \delta/2G \in \{0, \frac{1}{2}, 1, 10\}, H = 5$

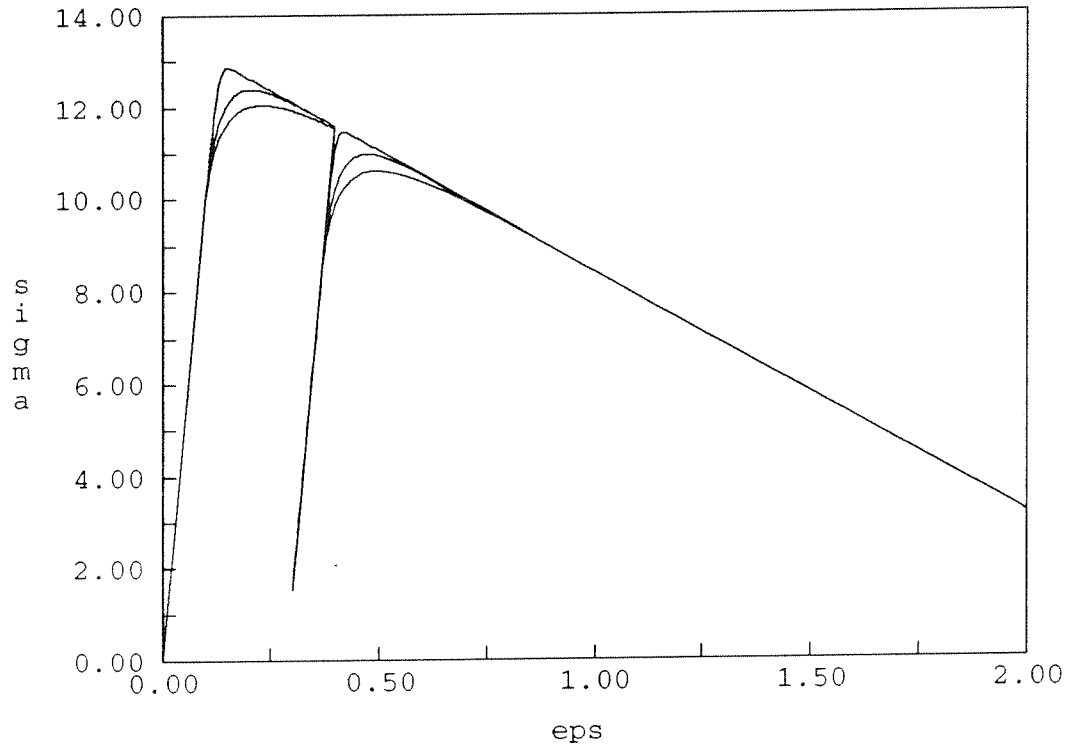

Figure 7: Uniaxial test: loading-unloading. $\beta = 3, \delta/2G \in \{\frac{1}{2}, 1, 10\}, H = -5$

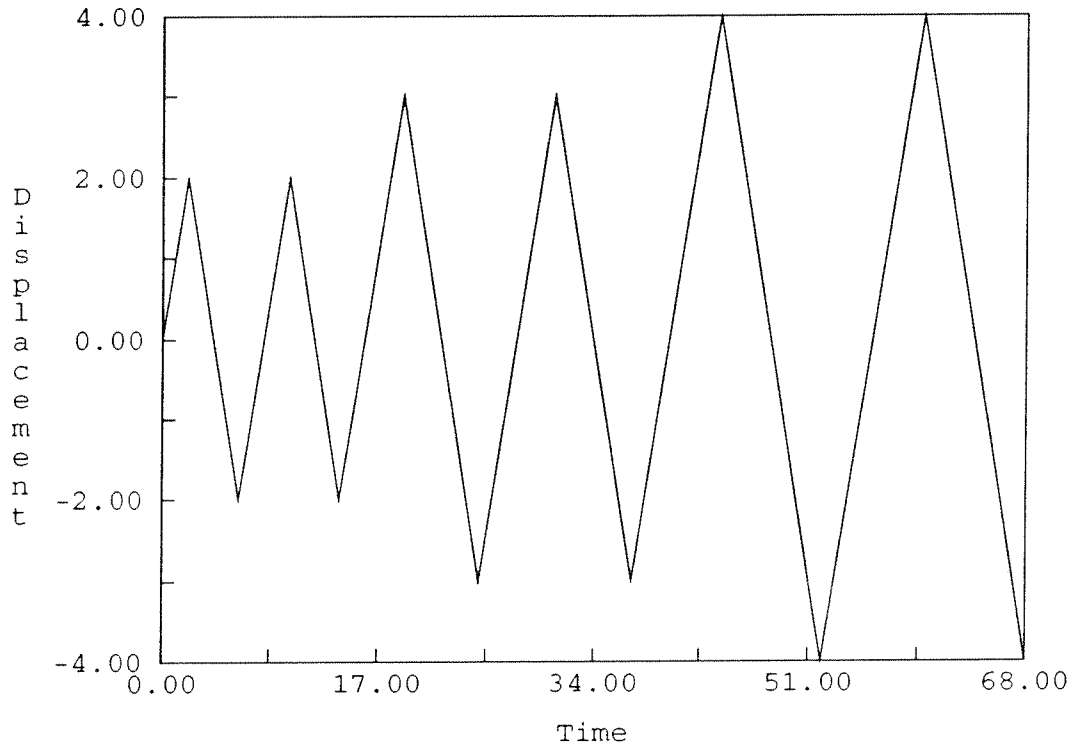

Figure 8: Uniaxial test: cyclic loading. Time history.

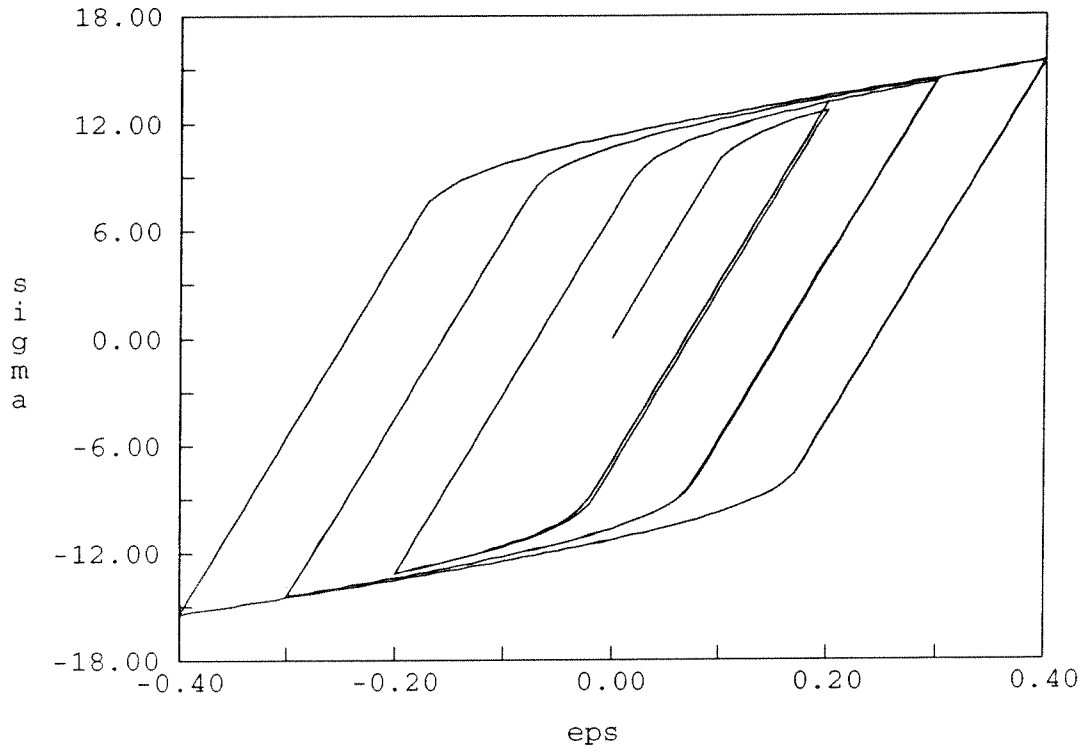

Figure 9: Uniaxial test: cyclic loading. $\beta = 3, \delta = G, H = 10$

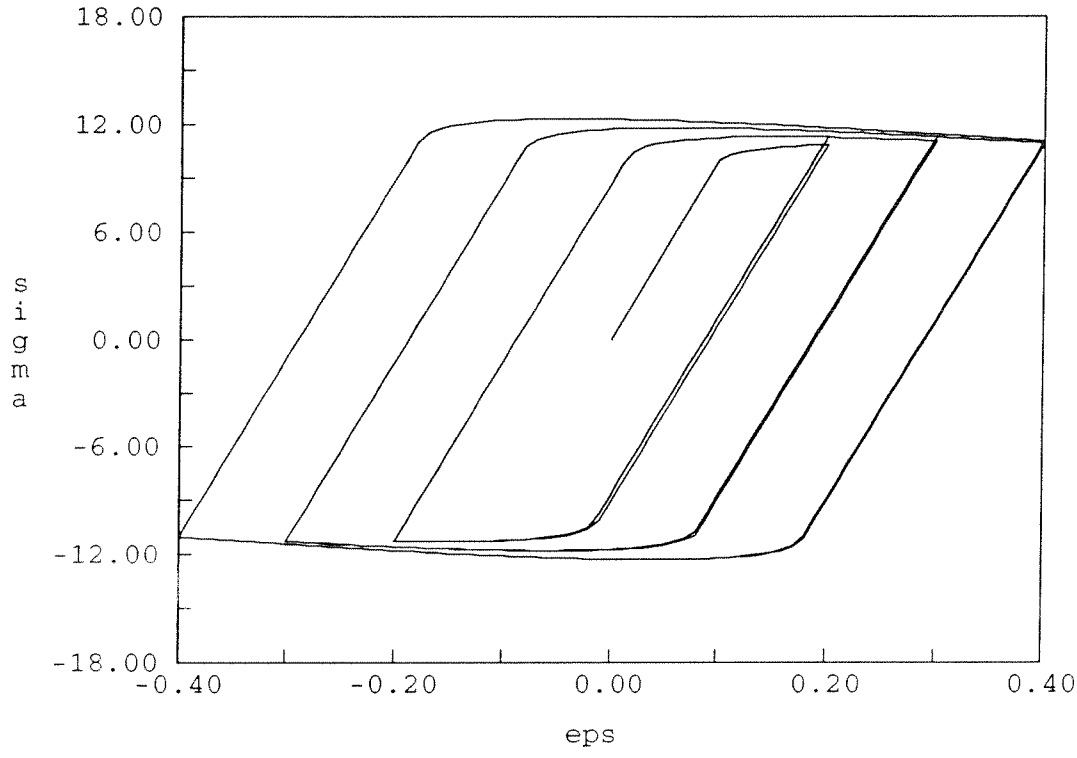

Figure 10: Uniaxial test: cyclic loading. $\beta = 3, \delta = G, H = -5$

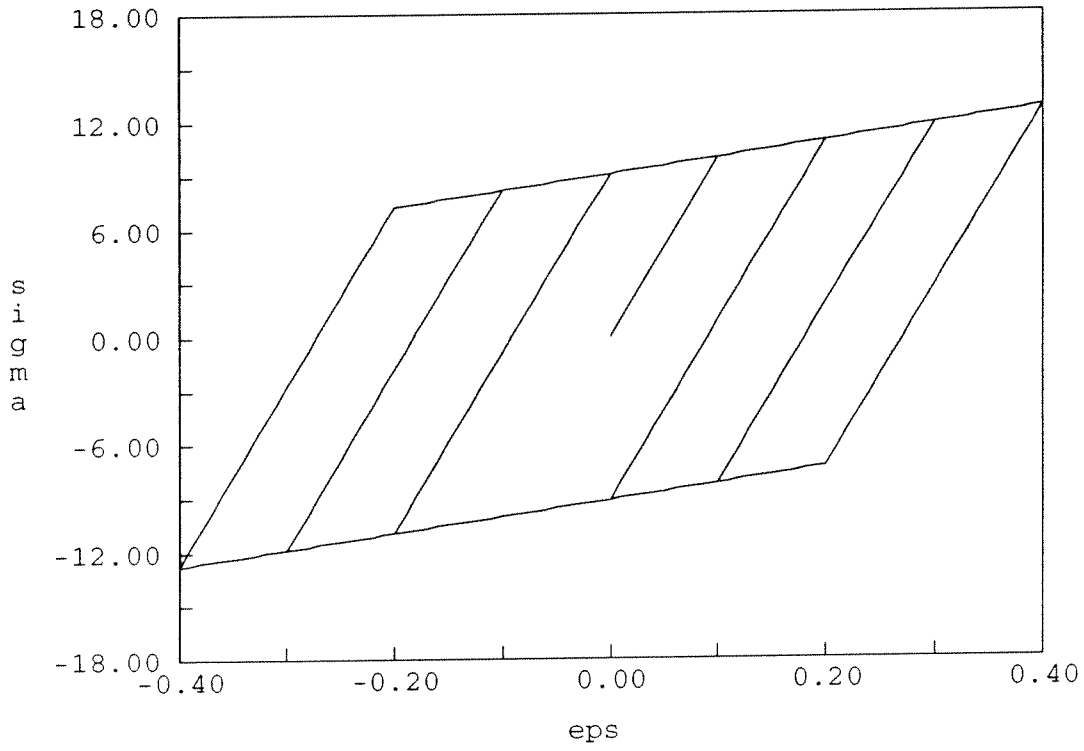

Figure 11: Uniaxial test: cyclic loading. Classical solution.

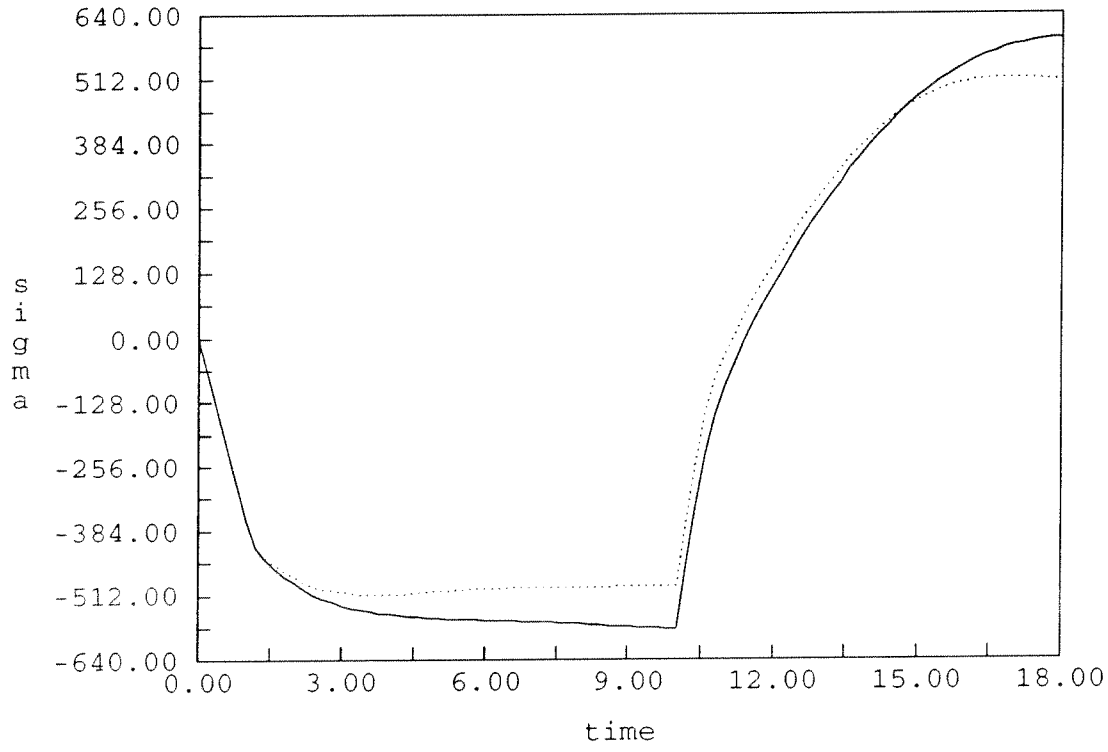

Figure 12: Thick walled tube under pressure. Radial stress versus time. For comparison, the solution from the classical model is also presented with a dotted line.

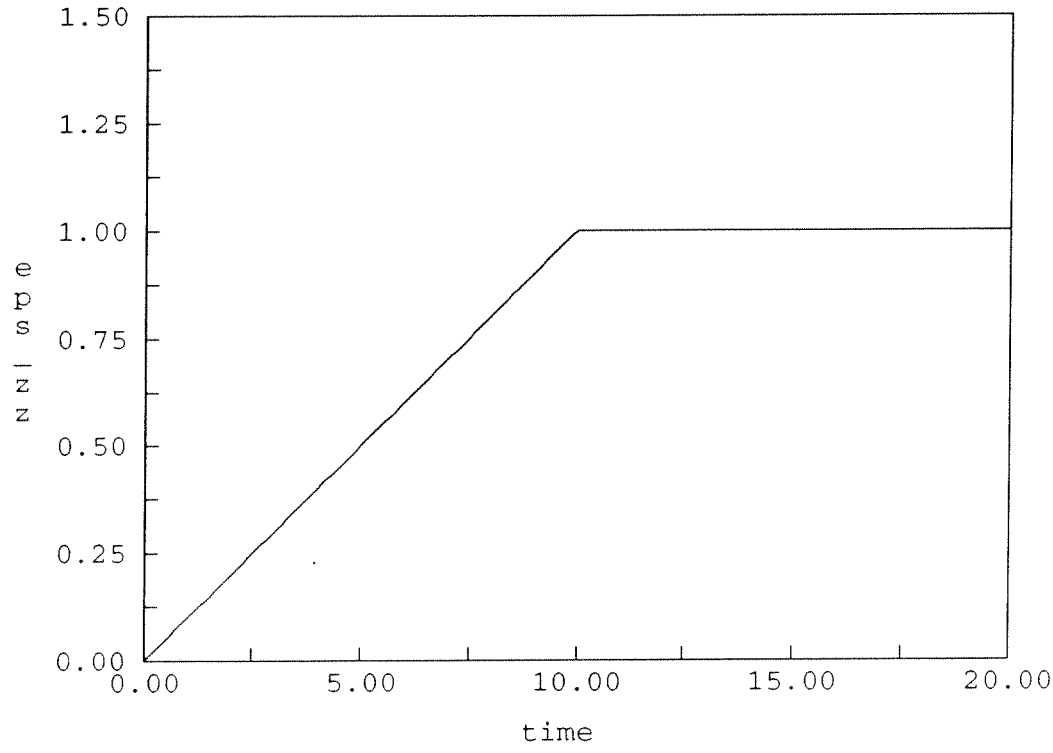

Figure 13: Thin walled tube in tension and torsion (displacement control). Load history in terms of the axial strain ϵ_{zz}.

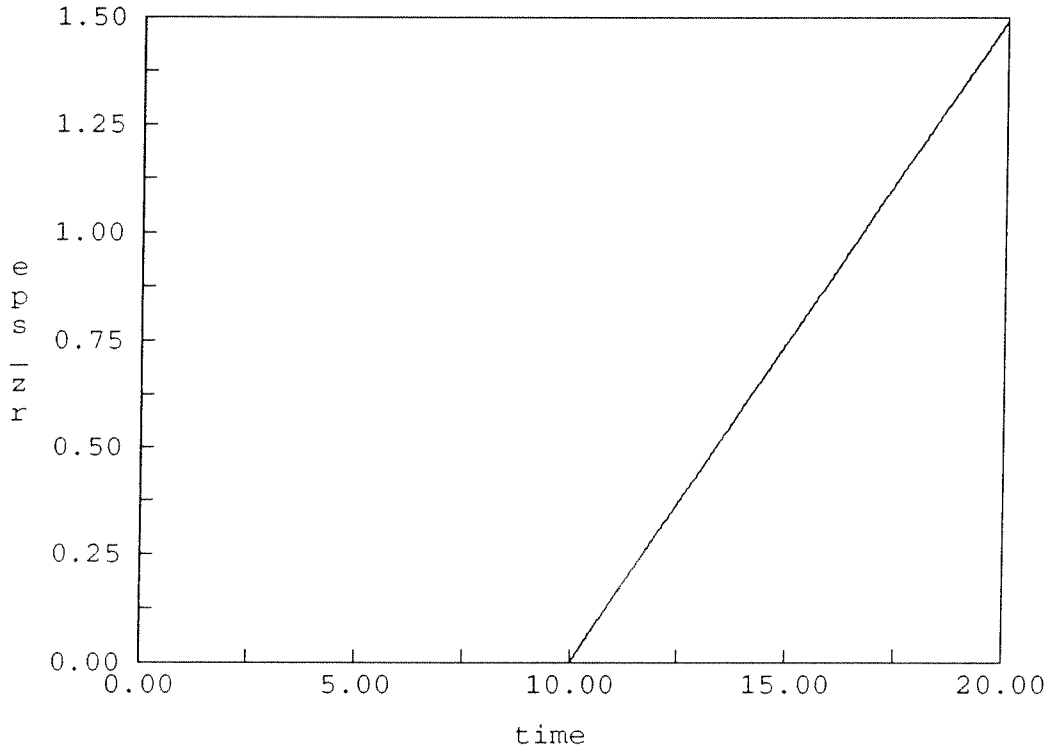

Figure 14: Thin walled tube in tension and torsion (displacement control). Load history in terms of the tangential strain $\gamma_{z\theta}$.

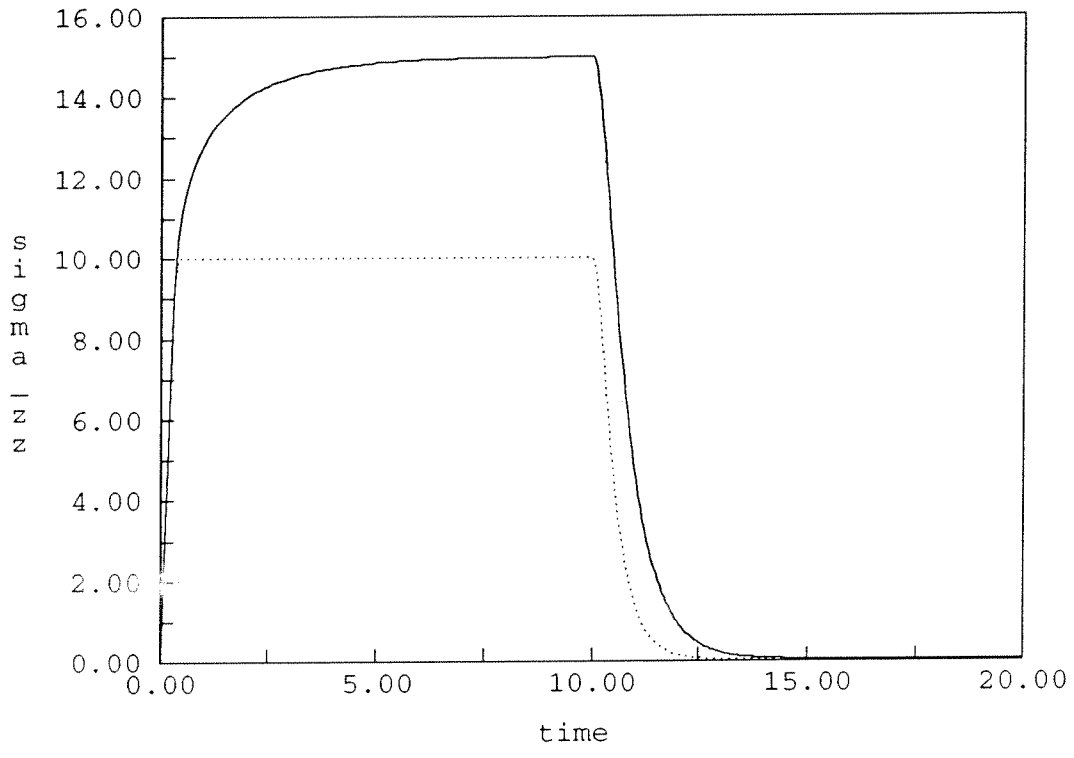

Figure 15: Thin walled tube in tension and torsion (displacement control). Normal stress σ_{zz} versus time. For comparison, the solution from the classical model is also presented with a dotted line.

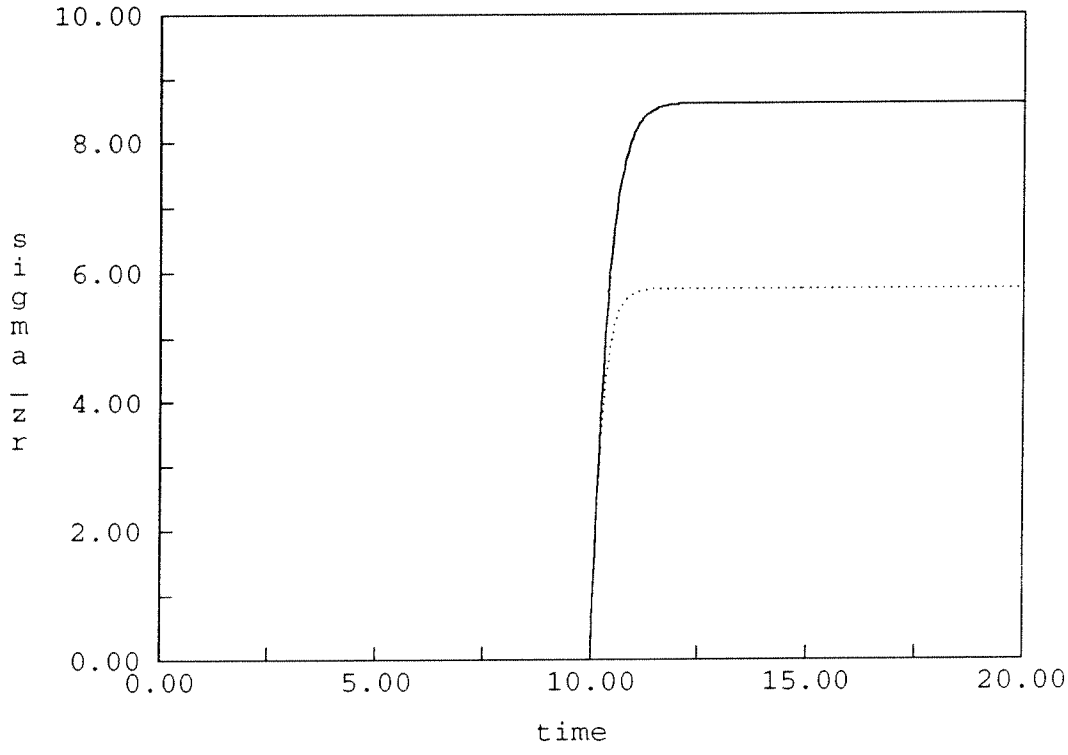

Figure 16: Thin walled tube in tension and torsion (displacement control). Tangential stress $\tau_{z\theta}$ versus time. For comparison, the solution from the classical model is also presented with a dotted line.

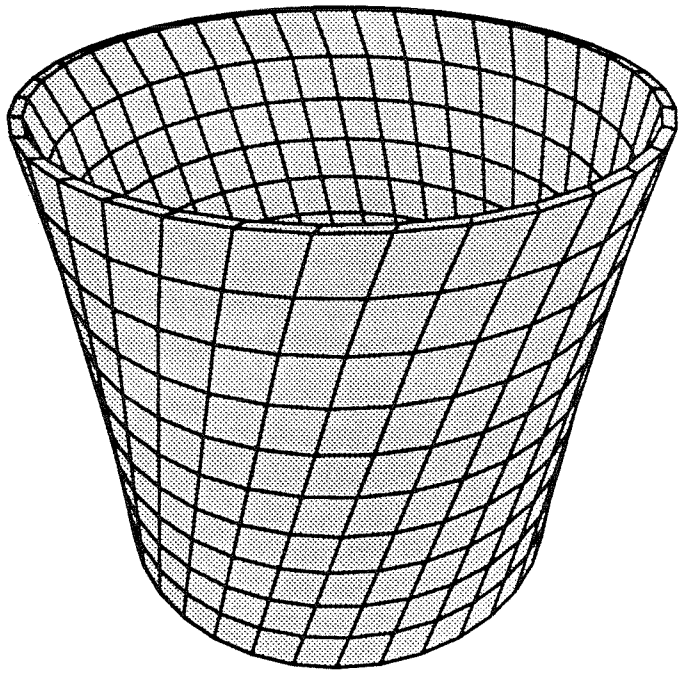

Figure 17: Thin walled tube in tension and torsion (displacement control). Three dimensional mesh at the end of the analysis.

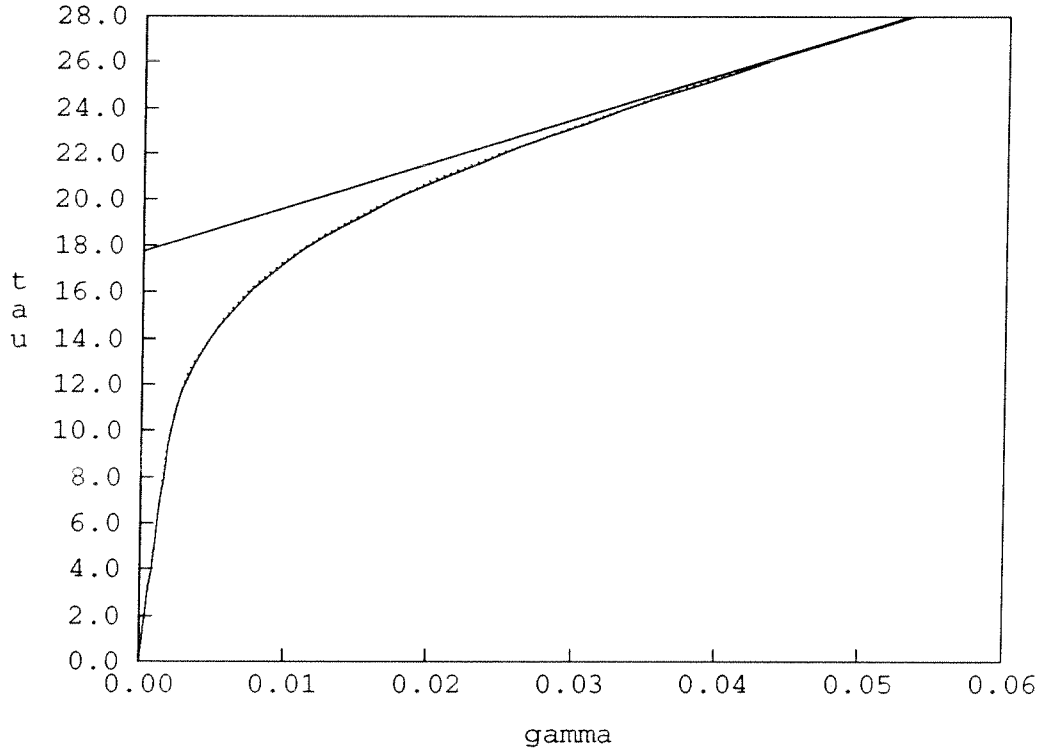

Figure 18: Thin walled tube in tension and torsion (stress control). Tangential stress $\sigma_{z\theta}$ versus tangential strain $\gamma_{z\theta}$ for $\bar{\sigma} = 0$
Analitycal solution: dotted line
Numerical solution: solid line

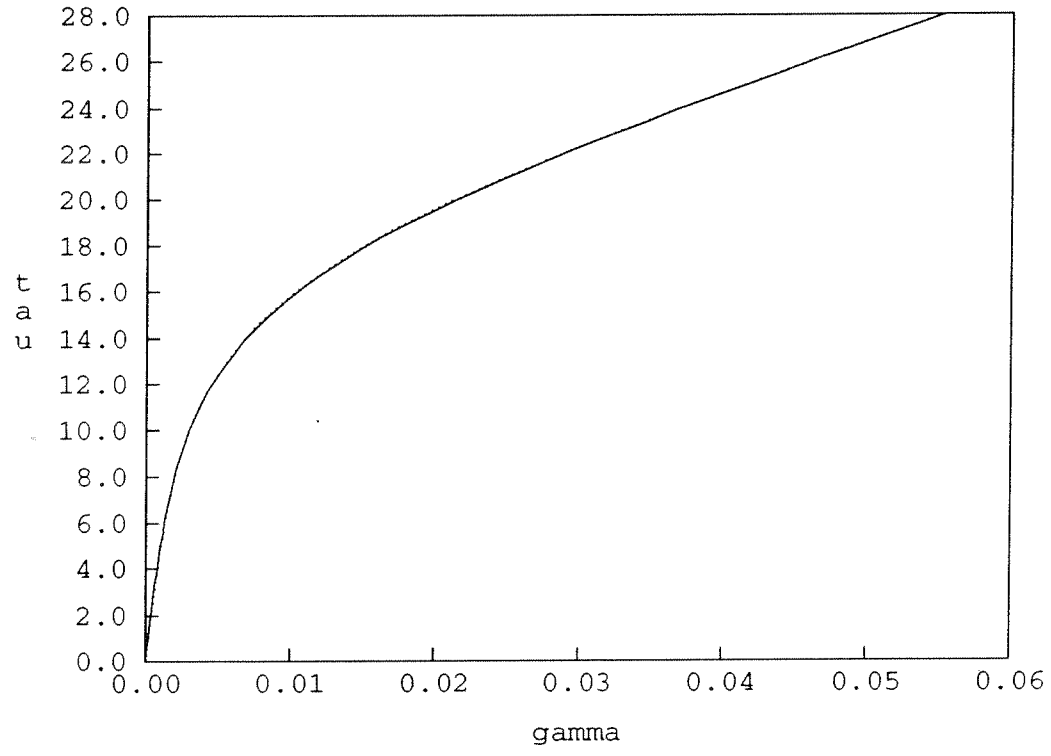

Figure 19: Thin walled tube in tension and torsion (stress control). Tangential stress $\sigma_{z\theta}$ versus tangential strain $\gamma_{z\theta}$ for $\bar{\sigma} = 16$
Analitycal solution: dotted line
Numerical solution: solid line

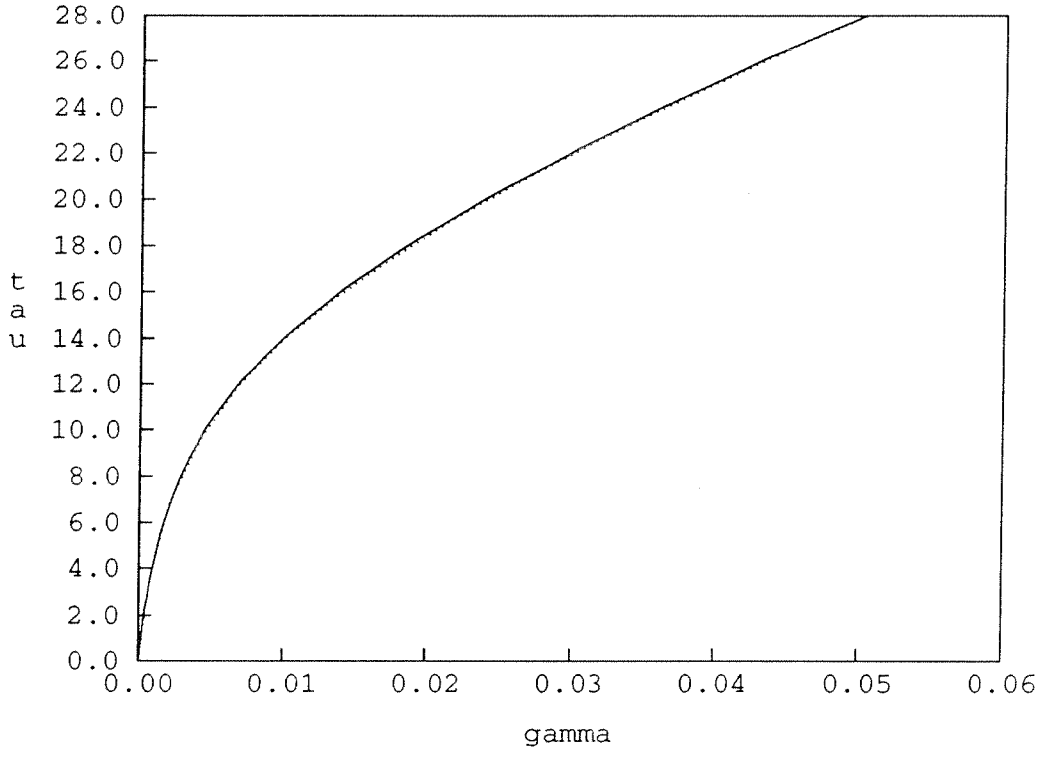

Figure 20: Thin walled tube in tension and torsion (stress control). Tangential stress $\sigma_{z\theta}$ versus tangential strain $\gamma_{z\theta}$ for $\bar{\sigma} = 32$
Analitycal solution: dotted line
Numerical solution: solid line

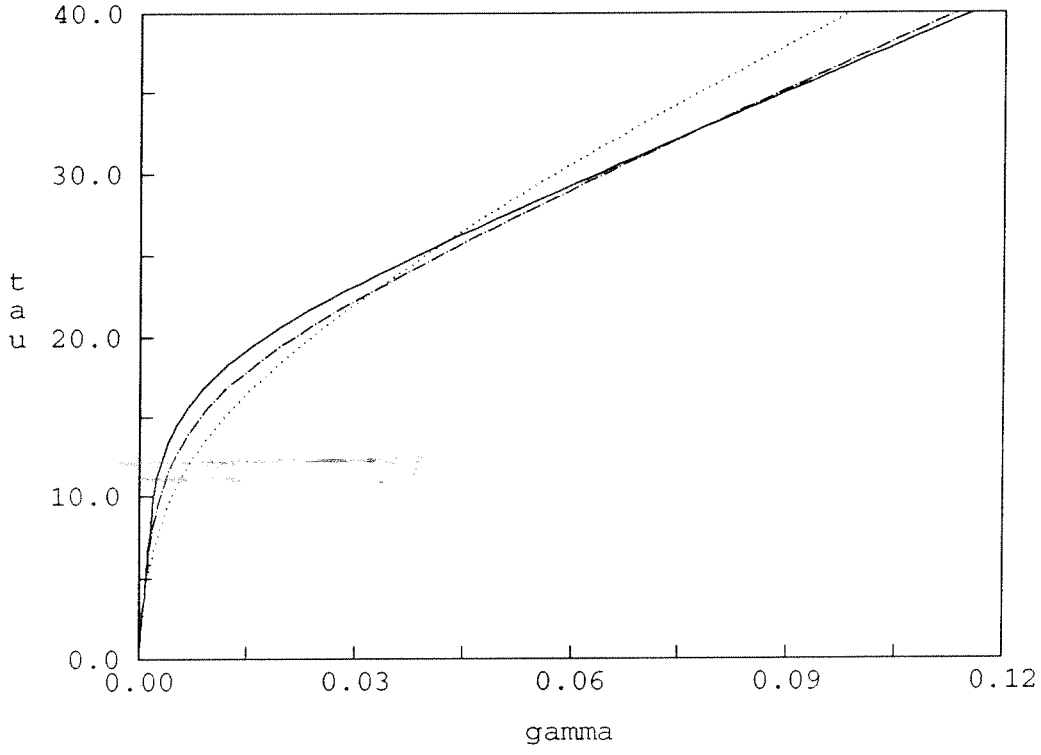

Figure 21: Thin walled tube in tension and torsion (stress control). Tangential stress $\sigma_{z\theta}$ versus tangential strain $\gamma_{z\theta}$ for $\bar{\sigma} \in \{0, 16, 32\}$
$\bar{\sigma} = 0$ solid line
$\bar{\sigma} = 16$ dot-dash line
$\bar{\sigma} = 32$ dotted line